686 *Inorg. Chem.* **2011**, *50*, 686–704
DOI: 10.1021/ic102256t

Inorganic Chemistry
Article

Homochiral, Helical Supramolecular Metal−Organic Frameworks Organized by Strong $\pi\cdots\pi$ Stacking Interactions: Single-Crystal to Single-Crystal Transformations in Closely Packed Solids

Daniel L. Reger,*,† Jacob J. Horger,† Mark D. Smith,† Gary J. Long,‡ and Fernande Grandjean§

†*Department of Chemistry and Biochemistry, University of South Carolina, Columbia, South Carolina 29208, United States* ,‡*Department of Chemistry, Missouri University of Science and Technology, University of Missouri, Rolla, Missouri 65409-0010, United States , and* §*Department of Physics, B5, University of Liège, B-4000 Sart-Tilman, Belgium*

Received November 9, 2010

Enantiopure, trifunctional carboxylate ligands synthesized by linking the strong $\pi\cdots\pi$ stacking 1,8-naphthalimide supramolecular synthon to three naturally occurring amino acids using the azide/alkyne click reaction have been prepared [amino acid = glycine ($\mathbf{L_{gly}}^-$), alanine ($\mathbf{L_{ala}}^-$), and serine ($\mathbf{L_{ser}}^-$)]. These ligands have been used to form complexes of the formula $[M(\mathbf{L_{amino\ acid}})_2(4,4'\text{-bipy})(H_2O)_2]\cdot xH_2O$ (M = Fe, Co, Ni, Cu, Zn; $x = 4.25-5.52$) when mixed with an appropriate metal salt and 4,4′-bipyridine by layering methods. These complexes are isostructural, with the central metal atom coordinated to two κ^1-carboxylate ligands, two water molecules, and one end each of two 4,4′-bipyridine ligands in a distorted octahedral environment. Each ligand is oriented in a trans arrangement. These complexes all have homochiral, helical, supramolecular, three-dimensional metal−organic framework structures, with the helical organization of the individual metallic units held together solely by strong, noncovalent $\pi\cdots\pi$ stacking interactions of the naphthalimide; the other two dimensions are organized mainly by the bipyridine ligands. The helices are extremely large; one turn of the helix travels ∼60 Å and has a diameter of ca. 40 Å. For the achiral ligand $\mathbf{L_{gly}}^-$, the nickel complex forms two types of homochiral crystals in the same tube, a clear example of spontaneous resolution. Despite the large size of the individual helices, they are tightly interconnected and nestled closely together. Part of the interconnection comes from the interstitial water molecules held inside the framework of the complexes in isolated pockets by hydrogen-bonding interactions. For both $[Cu(\mathbf{L_{ala}})_2(4,4'\text{-bipy})(H_2O)_2]\cdot 4.25H_2O$ and $[Co(\mathbf{L_{ser}})_2(4,4'\text{-bipy})(H_2O)_2]\cdot 4.68H_2O$, the interstitial water molecules can be removed by placing the crystals under a vacuum for several hours, a process that can be reversed by exposure to atmospheric moisture. This removal/reintroduction of the interstitial water molecules takes place with no loss of crystallinity, representing dramatic examples of single-crystal to single-crystal transformations. The structures undergo little change other than the pockets holding the interstitial water molecules in the hydrated complexes become void spaces in the dehydrated complexes. The removal/reintroduction of the water molecules in these closely packed solids is facilitated by the "soft" $\pi\cdots\pi$ stacking interactions organizing one dimension of the structures. The observed magnetic and Mössbauer spectral properties are typical of isolated, magnetically dilute, paramagnetic pseudooctahedral divalent transition-metal complexes.

Introduction

An important area of inorganic chemistry for many decades has been the synthesis and structural study of the broad class of compounds referred to as inorganic frameworks.[1−4] These complexes are important for use as catalysts,[5] molecular sensors,[6] and molecular sieves[7] and in the

*To whom correspondence should be addressed. E-mail: reger@chem.sc.edu.

(1) Robson, R. *Dalton Trans*. **2008**, 5113–5131.
(2) Tranchemontagne, D. J.; Mendoza-Cortes, J. L.; O'Keeffe, M.; Yaghi, O. M. *Chem. Soc. Rev*. **2009**, *38*, 1257–1283.
(3) Rowsell, J. L. C.; Yaghi, O. M. *Microporous Mesoporous Mater*. **2004**, *73*, 3–14.
(4) Férey, G. *Chem. Soc. Rev*. **2008**, *37*, 191–214.
(5) (a) Corma, A.; García, H.; Llabrés i Xamena, F. X. *Chem. Rev*. **2010**, *110*, 4606−4655. (b) Farrusseng, D.; Aguado, S.; Pinel, C. *Angew. Chem., Int. Ed*. **2009**, *48*, 7502–7513. (c) Tanabe, K. K.; Cohen, S. M. *Inorg. Chem*. **2010**, *49*, 6766–6774. (d) Lin, W. *Top. Catal*. **2010**, *53*, 869–875.
(6) (a) Chen, B.; Xiang, S.; Qian, G. *Acc. Chem. Res*. **2010**, *43*, 1115−1124. (b) Liu, S.; Li, J.; Luo, F. *Inorg. Chem. Commun*. **2010**, *13*, 870–872. (c) Green, M. A. *Nat. Mater*. **2010**, *9*, 539–540. (d) Lan, A.; Li, K.; Wu, H.; Olson, D.; Emge, T.; Ki, W.; Hong, M.; Li, J. *Angew. Chem., Int. Ed*. **2009**, *48*, 2334–2338. (e) Chen, B.; Wang, L.; Zapata, F.; Qian, G.; Lobkovsky, E. B. *J. Am. Chem. Soc*. **2008**, *130*, 6718–6719. (f) Chen, B.; Wang, L.; Xiao, Y.; Fronczek, F.; Xue, M.; Cui, Y.; Qian, G. *Angew. Chem., Int. Ed*. **2009**, *48*, 500–503.
(7) (a) Lee, H.; Zones, S. I.; Davis, M. E. *Nature* **2003**, *425*, 385–388. (b) Corma, A. *Chem. Rev*. **1997**, *97*, 2373–2420 and references cited therein. (c) Czaja, A. U.; Trukhan, N.; Muller, U. *Chem. Soc. Rev*. **2009**, *38*, 1284–1293 and references cited therein.

 Published on Web 12/09/2010

design of materials with interesting physical properties, such as magnetism.[8] Many different types of interactions organize these frameworks, some with high and others with lower bonding energies.

The zeolites, which are purely inorganic frameworks, were the first to be extensively studied.[9] More recently, using zeolites as the model, the inorganic building blocks in the zeolite frameworks have been replaced by organic ligands in one, two, or all three dimensions.[10] The chemistry of the latter class of compounds, where single metal ions or small clusters of metal ions are linked by multifunctional organic ligands, has exploded in the last 20 years because, by changing the characteristics of the metal ion "nodes" and the organic ligands, one can build virtually any desired architecture.[1−3]

Systems built with metal ion nodes and linking organic ligands have been called either coordination polymers[1] or, more recently, metal−organic frameworks (MOFs).[2,3] Yaghi and co-workers have distinguished the two terms by arguing that coordination polymers are linked by classic metal (M)−donor atom bonds (where the donor atom is from ligands such as an amine or pyridine) that are relatively weak, whereas MOFs are built on donor groups such as chelating carboxylates that have stronger M−donor atom linkages.[3] Both classes of complexes have highly organized structures, but different systems can have a range of M−donor atom bond strengths.

Highly organized structures both with and without metal ions can also be built partially or completely with supramolecular interactions, where "supramolecular" refers to the chemistry beyond the covalent bond.[11] Here again, a variety of supramolecular architectures have been synthesized with a large range of bonding forces; depending on the systems, the interactions can range from classic M−donor atom bonds, to strong halogen[12] or hydrogen bonds,[13] to much weaker forces such as weak hydrogen bonds[14] and $\pi\cdots\pi$ stacking of small aromatics.[15]

We have been preparing metal ion complexes from bifunctional ligands, initially based on poly(pyrazolyl)borate and poly(pyrazolyl)methane donor groups, that also contain groups designed to enter into strong supramolecular interactions.[16] We have recently focused on the 1,8-naphthalimide supramolecular

Chart 1

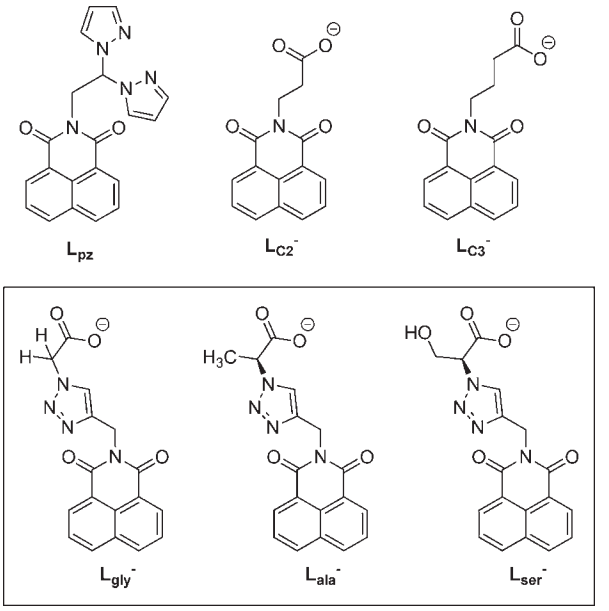

synthon for two reasons: its tendency to form very strong $\pi\cdots\pi$ stacking interactions and the ease with which it can be introduced from amine-bearing ligands and 1,8-naphthalic anhydride. We have demonstrated these advantages by preparing a number of bifunctional ligands bearing both the 1,8-naphthalimide moiety and appropriate donor groups ($\mathbf{L_{pz}}$, $\mathbf{L_{C2}}^-$, and $\mathbf{L_{C3}}^-$; Chart 1). In our initial work with the bis(pyrazolyl)methane ligand $\mathbf{L_{pz}}$, metal complexes that were dimeric[17] as well as those with more complex structures that could be described as coordination polymers[18] were prepared. We were able to show that the dimeric systems, held together only by the $\pi\cdots\pi$ stacking interaction in the solid-state structures remained dimeric in solution, as demonstrated by NMR diffusion experiments.[17]

Given the strength of the $\pi\cdots\pi$ stacking interactions of the 1,8-naphthalimide group demonstrated in our initial work,[17] we have prepared the bifunctional carboxylate ligands $\mathbf{L_{C2}}^-$ and $\mathbf{L_{C3}}^-$ shown in Chart 1 with the objective of making MOF-type structures but ones that were supported in at least one dimension by supramolecular strong $\pi\cdots\pi$ stacking interactions. While many structurally rigid MOF frameworks have been reported,[1−3] the rational design of more flexible but still crystalline structures is an area with much less activity.[19−21] These types of structures have the potential to change their properties when lattice guests are introduced or removed.

Our first publication with these two ligands, using copper(II) carboxylate dimers as the central metal core, demonstrated that this approach can lead to highly organized structures.[22] For example, by combining $\mathbf{L_{C2}}^-$ with the linking ligand

(8) (a) Maspoch, D.; Ruiz-Molina, D.; Veciana, J. *J. Mater. Chem.* **2004**, *14*, 2713–2723 and references cited therein. (b) Kurmoo, M. *Chem. Soc. Rev.* **2009**, *38*, 1353–1379 and references cited therein. (c) Inoue, K.; Imai, H.; Ghalsasi, P. S.; Kikuchi, K.; Ohba, M.; Ōkawa, H.; Yakhmi, J. V. *Angew. Chem., Int. Ed.* **2001**, *40*, 4242–4245. (d) Armentano, D.; De Munno, G.; Lloret, F.; Palii, A. V.; Julve, M. *Inorg. Chem.*. **2002**, *41*, 2007–2013. (e) Gao, E.; Bai, S.; Wang, Z.; Yan, C. *J. Am. Chem. Soc.* **2003**, *125*, 4984–4985. (f) Inoue, K.; Kikuchi, K.; Ohba, M.; Ōkawa, H. *Angew. Chem., Int. Ed.* **2003**, *42*, 4810–4813.

(9) Cheetham, A. K.; Férey, G.; Loiseau, T. *Angew. Chem., Int. Ed.* **1999**, *38*, 3268–3292.

(10) Férey, G. *Chem. Mater.* **2001**, *13*, 3084–3098.

(11) Lehn, J.-M. *Angew. Chem., Int. Ed.* **1988**, *27*, 89–112.

(12) Bertani, R.; Sgarbossa, P.; Venzo, A.; Lelj, F.; Amati, M.; Resnati, G.; Pilati, T.; Metrangolo, P.; Terraneo, G. *Coord. Chem. Rev.* **2010**, *254*, 677–695.

(13) Ingleson, M. J.; Bacsa, J.; Rosseinsky, M. J. *Chem. Commun.* **2007**, 3036–3038.

(14) (a) Desiraju, G. R. *Chem. Commun.* **2005**, 2995–3001. (b) García-Báez, E. V.; Martínez-Martínez, F. J.; Höpfl, H.; Padilla-Martínez, I. I. *Cryst. Growth Des.* **2003**, *3*, 35–45.

(15) (a) Janiak, C. *Dalton Trans.* **2000**, 3885–3896. (b) Claessens, C. G.; Stoddart, J. F. *J. Phys. Org. Chem.* **1997**, *10*, 254–272. (c) Guo, H.; Guo, X.; Batten, S. R.; Song, J.; Song, S.; Dang, S.; Zheng, G.; Tang, J.; Zhang, H. *Cryst. Growth Des.* **2009**, *9*, 1394–1401.

(16) (a) Reger, D. L.; Sirianni, E.; Horger, J. J.; Smith, M. D.; Semeniuc, R. F. *Cryst. Growth Des.* **2010**, *10*, 386–393. (b) Reger, D. L.; Gardinier, J. R.; Elgin, J. D.; Smith, M. D.; Hautot, D.; Long, G. J.; Grandjean, F. *Inorg. Chem.* **2006**, *45*, 8862–8875.

(17) (a) Reger, D. L.; Elgin, J. D.; Semeniuc, R. F.; Pellechia, P. J.; Smith, M. D. *Chem. Commun.* **2005**, 4068–4070. (b) Reger, D. L.; Elgin, J. D.; Pellechia, P. J.; Smith, M. D.; Simpson, B. K. *Polyhedron* **2009**, *28*, 1469–1474.

(18) Reger, D. L.; Semeniuc, R. F.; Elgin, J. D.; Rassolov, V.; Smith, M. D. *Cryst. Growth Des.* **2006**, *6*, 2758–2768.

(19) Serre, C.; Surble, S.; Mellot-Draznieks, C.; Filinchuk, Y.; Férey, G. *Dalton Trans.* **2008**, 5462–5464.

(20) Wang, Z.; Cohen, S. M. *J. Am. Chem. Soc.* **2009**, *131*, 16675–16677.

(21) Fukushima, T.; Horike, S.; Inubushi, Y.; Nakagawa, K.; Kubota, Y.; Takata, M.; Kitagawa, S. *Angew. Chem., Int. Ed.* **2010**, *49*, 4820–4824.

(22) Reger, D. L.; Debreczeni, A.; Reinecke, B.; Rassolov, V.; Smith, M. D.; Semeniuc, R. F. *Inorg. Chem.* **2009**, *48*, 8911–8924.

4,4′-bipyridine in the preparation of copper carboxylate dimers, we prepared $[Cu_2(\mathbf{L_{C2}})_4(bipy)]$, a complex that has a three-dimensional structure in which the 1,8-naphthalimide groups overlap to form one-dimensional ribbons, with the second dimension formed by the coordinate−covalent bonds of the 4,4′-bipyridine ligands and the third dimension linked by mechanical interlocking.

In order to extend this chemistry to the syntheses of flexible *chiral* framework solids, we have prepared the analogous *trifunctional* ligands that contain the 1,8-naphthalimide synthon coupled to naturally occurring amino acids. A number of readily available chiral ligands,[23] the simplest of which are amino acids,[24] have been studied in coordination chemistry. While the synthesis of chiral framework structures has been an area of significant recent interest for a multitude of potential applications,[25−27] the use of simple amino acids coupled to the strong $\pi\cdots\pi$ stacking naphthalimide group represents a new direction for these studies.

In our first approach, we have linked the naphthalimide group to three naturally occurring amino acids using the azide/alkyne "click" reaction so as to place a flexible, enantiopure spacer between the donor atoms and the supramolecular synthon, ligands $\mathbf{L_{gly}}^-$, $\mathbf{L_{ala}}^-$, and $\mathbf{L_{ser}}^-$ in Chart 1. We anticipated that the enantiopure center (not for $\mathbf{L_{gly}}^-$) would "project" its chirality to support homochiral helical structures that have highly organized frameworks partially supported by the supramolecular synthon. A particularly attractive aspect of this and our earlier carboxylate chemistry is that we are preparing neutral complexes, so we can study the structure without any interference from counterions. Reported here are synthetic, structural, magnetic, and Mössbauer studies of a family of such complexes where the metal ion is varied along the first-row transition metals from iron to zinc, using the three different ligands, which all yield surprisingly similar structures. The use of the $\pi\cdots\pi$ stacking interaction as part of the framework construction has led to closely packed homochiral, helical solids that show interesting single-crystal to single-crystal transformations. We have previously communicated some of these results.[28]

Experimental Section

General Considerations. Unless otherwise specified, all operations were carried out with no special precautions to exclude air or moisture. All solvents and reagents were used as purchased. *N*-Propargylnaphthalimide was prepared according to a known procedure.[29]

The magnetic properties have been measured in the solid state with a Quantum Design MPMSXL superconducting quantum interference magnetometer. Gelatin capsules designed to prevent sample movement were used as sample containers. The magnetic properties were first obtained upon field cooling from 300 K to either 2 or 5 K in a 0.05 or 0.1 T direct-current applied field followed by subsequent warming to 300 K. For each complex, there was no significant difference between the moments obtained upon cooling and subsequent warming, and the moments have been merged. The molar magnetic susceptibilities have been corrected for diamagnetism by using Pascal's constants; the exact fields and corrections are given in a subsequent table. The details of the fitting procedures used to understand the magnetic properties of each of the complexes are given in the text and Supporting Information. The statistical errors associated with the fits of the magnetic data are given in the text and figure captions. The actual errors in the reported parameters may be larger than the statistical errors because of the errors associated with the sample mass, the loss of solvation molecules, the difficulty in determining the best diamagnetic corrections from Pascal's constants, and the correction for the capsule contribution to the observed magnetic moment.

The Mössbauer spectra of $[Fe(\mathbf{L_{ala}})_2(4,4'\text{-bipy})(H_2O)_2]\cdot 4.84H_2O$ have been measured between 85 and 295 K on a constant-acceleration spectrometer that utilized a 295 K rhodium matrix cobalt-57 source and was calibrated at 295 K with α-iron powder. The spectra have been obtained with an absorber that contained 12 mg/cm^2 of the sample that had been crushed but not ground and dispersed in boron nitride powder. The observed spectra have been fit with two symmetric quadrupole doublets, and the estimated relative errors are ±0.005 mm/s for the isomer shifts, ±0.01 mm/s for the quadrupole splittings and line widths, and ±0.005 mm/s (% ε) for the spectral absorption areas. The absolute errors are approximately twice as large.

Potassium (*S*)-2-[4-[(1,8-Naphthalamido)methyl]-1*H*-1,2,3-triazolyl]propanoate ($\mathbf{KL_{ala}}$). Imidazole-1-sulfonyl azide hydrochloride[30] (5.00 g, 24 mmol), K_2CO_3 (1.78 g, 20 mmol), and L-alanine (1.78 g, 20 mmol) were stirred together in 100 mL of dry methanol. $CuSO_4$ (200 mg, 0.80 mmol) was added, and the mixture was stirred for 24 h. A solution of sodium ascorbate (1.59 g, 8.0 mmol) dissolved in 80 mL of water was added, followed by *N*-propargylnaphthalimide (4.23 g, 18 mmol) and 100 mL of acetone. This suspension was stirred for a further 24 h and then concentrated to a volume of approximately 80 mL by rotary evaporation. The residue was diluted with water until it became clear and then was acidified by the careful dropwise addition of 3 M HCl. The product, $\mathbf{HL_{ala}}$, was isolated by suction filtration, washed well

(23) (a) Hoshino, Y.; Yamamoto, H. *J. Am. Chem. Soc.* **2000**, *122*, 10452–10453. (b) Lee, S. J.; Lin, W. *Acc. Chem. Res.* **2008**, *41*, 521–537. (c) Dangel, B.; Clarke, M.; Haley, J.; Sames, D.; Plot, R. *J. Am. Chem. Soc.* **1997**, *119*, 10865. (d) Corey, E. J.; Shibata, S.; Bakshi, R. K. *J. Org. Chem.* **1988**, *53*, 2861–2863.

(24) (a) Zhabg, Y.; Saha, M. K.; Bernal, I. *CrystEngComm* **2002**, *5*, 34–37. (b) Anokhina, E. V.; Go, Y. B.; Lee, Y.; Vogt, T.; Jacobson, A. J. *J. Am. Chem. Soc.* **2006**, *128*, 9957. (c) Mizutani, M.; Maejima, N.; Jitsukawa, K.; Masuda, H.; Einaga, H. *Inorg. Chim. Acta* **1998**, *283*, 105. (d) Doyle, M. P.; Zhou, Q.; Charnsangavej, C.; Longoria, M. A. *Tetrahedron Lett.* **1996**, *37*, 4129–4132. (e) Davies, H. M. L.; Bruzinski, P. R.; Fall, M. *Tetrahedron Lett.* **1996**, *37*, 4133–4136. (f) Hashimoto, S.; Watanabe, N.; Ikegami, S. *Tetrahedron Lett.* **1990**, *31*, 5173–5174. (g) Zhang, Y.; Saha, M. K.; Bernal, I. *CrystEngComm* **2003**, *5*, 34–37. (h) Xie, Y.; Xiong, R.; Xue, X.; Chen, X.; Xue, Z.; You, X. *Inorg. Chem.* **2002**, *41*, 3323–3326.

(25) (a) Lin, W. *J. Solid State Chem.* **2005**, *178*, 2486–2490. (b) Seo, J. S.; Whang, D.; Lee, H.; Jun, S. I.; Oh, J.; Jeon, Y. J.; Kim, K. *Nature* **2000**, *404*, 982–986. (c) Bradshaw, D.; Prior, T. J.; Cussen, E. J.; Claridge, J. B.; Rosseinsky, M. J. *J. Am. Chem. Soc.* **2004**, *126*, 6106–6114. (d) Xiong, R.; You, X.; Abrahams, B. F.; Xue, Z.; Che, C. *Angew. Chem., Int. Ed.* **2001**, *40*, 4422–4425.

(26) (a) Kurmoo, M.; Kumagai, H.; Akita-Tanaka, M.; Inoue, K.; Takagi, S. *Inorg. Chem.* **2006**, *45*, 1627–1637. (b) Zeng, M.; Wang, B.; Wang, X.; Zhang, W.; Chen, X.; Gao, S. *Inorg. Chem.* **2006**, *45*, 7069–7076. (c) Gu, Z.; Zhou, X.; Jin, Y.; Xiong, R.; Zuo, J.; You, X. *Inorg. Chem.* **2007**, *46*, 5462–5464. (d) Ashiry, K. O.; Zhao, Y.; Shao, K.; Su, Z.; Fu, Y.; Hao, X. *Inorg. Chem. Commun.* **2008**, *11*, 1181–1183. (e) Rikken, G. L.; Raupach, E. *Nature* **1997**, *390*, 493–494. (f) Rikken, G. L.; Raupach, E. *Nature* **2000**, *405*, 932–935. (g) Andrés, R.; Brissard, M.; Gruselle, M.; Train, C.; Vaissermann, J.; Malézieux, B.; Jamet, J.; Verdaguer, M. *Inorg. Chem.* **2001**, *40*, 4633–4640.

(27) (a) Bodwin, J. J.; Pecoraro, V. L. *Inorg. Chem.* **2000**, *39*, 3434–3435. (b) Bodwin, J. J.; Cutland, A. D.; Malkani, R. G.; Pecoraro, V. L. *Coord. Chem. Rev.* **2001**, *216−217*, 489–512. (c) Yuan, G.; Shao, K.; Wang, X.; Lan, Y.; Du, D.; Su, Z. *CrystEngComm* **2010**, *12*, 1147–1152. (d) Yu, J.; Xu, R. *J. Mater. Chem.* **2008**, *18*, 4021–4030. (e) Frischmann, P. D.; Facey, G. A.; Ghi, P. Y.; Gallant, A. J.; Bryce, D. L.; Lelj, F.; MacLachlan, M. *J. Am. Chem. Soc.* **2010**, *132*, 3893–3908. (f) Liu, T.; Liu, Y.; Xuan, W.; Cui, Y. *Angew. Chem., Int. Ed.* **2010**, *49*, 4121–4124. (g) Sahoo, S.; Ray, M. *Chem.—Eur. J.* **2010**, *16*, 5004–5007. (h) Hao, H.; Liu, W.; Tan, W.; Lin, Z.; Tong, M. *Cryst. Growth Des.* **2009**, *9*, 457–465. (i) Yuan, G.; Zhu, C.; Xuan, W.; Cui, Y. *Chem.—Eur. J.* **2009**, *15*, 6428–6434.

(28) Reger, D. L.; Horger, J.; Smith, M. D.; Long, G. J. *Chem. Commun.* **2009**, 6219–6221.

(29) Walser, A.; Flynn, T.; Mason, C.; Crowley, H.; Maresca, C.; Yaremko, B.; O'Donnell, M. *J. Med. Chem.* **1991**, *34*, 1209–1221.

(30) Goddard-Borger, E. D.; Stick, R. V. *Org. Lett.* **2007**, *9*, 3797–3800.

with water, and dried overnight in vacuo to yield 5.89 g (93% yield, based on *N*-propargylnaphthalimide) of an insoluble white solid. A powdered sample of this solid (3.50 g, 10 mmol) was stirred for 1 h with a stoichiometric amount of 1 M methanolic KOH (10 mL, 10 mmol). Additional methanol was then added to dissolve the ligand (total volume ca. 275 mL), the solution was filtered through a short plug of Celite to remove traces of insoluble impurities, and the solvent was then removed by rotary evaporation to yield $\mathbf{KL_{ala}}$ as an off-white solid in quantitative yield (3.88 g, 10 mmol). $[\alpha]^{20}_D$: +3.77° (*c* 1.0 M MeOH). ^{1}H NMR (CD_3OD): δ 1.73 (d, J = 7.3 Hz, 3H, β-C*H*$_3$), 5.14 (q, J = 7.3 Hz, 1H, α-C*H*), 5.43 (s, 2H, C*H*$_2$), 7.76 (t, J = 8.2 Hz, 2H, nphth), 8.00 (s, 1H, triazole), 8.29 (d, J = 8.5 Hz, 2H, nphth), 8.52 (d, J = 4.1 Hz, 2H, nphth). ES$^-$-MS for $\{C_{18}H_{13}N_4O_4\}^-$: calcd, 349.0937; obsd, 349.0944. Anal. Calcd for $C_{18}H_{13}N_4O_4K$: C, 55.66; H, 3.37; N, 14.42. Found: C, 55.50; H, 3.22; N, 14.39.

Potassium (*S*)-2-[4-[(1,8-Naphthalamido)methyl]-1*H*-1,2,3-triazolyl]3-hydroxypropanoate ($\mathbf{KL_{ser}}$). This compound was prepared via the same procedure as that for $\mathbf{KL_{ala}}$ using L-serine (2.10 g, 20 mmol). The precipitation with 3 M HCl afforded 6.95 g (85% yield) of $\mathbf{HL_{ser}}$. This product (3.66 g, 10 mmol) was treated with 1 M methanolic KOH in the same manner as $\mathbf{HL_{ala}}$ to give $\mathbf{KL_{ser}}$ in quantitative yield (4.04 g, 10 mmol). $[\alpha]^{20}_D$: +4.81° (*c* 1.0 M MeOH). ^{1}H NMR (CD_3OD): δ 3.98 (m, 2H, β-C*H*$_2$), 5.20 (d, J = 3.8 Hz, 1H, α-C*H*), 5.44 (s, 2H, C*H*$_2$), 7.74 (dd, J = 7.3 and 8.4 Hz, 2H, 3-nphth), 8.10 (s, 1H, triazole), 8.26 (dd, J = 0.9 and 8.2 Hz, 2H, 4-nphth), 8.49 (dd, J = 0.9 and 7.3 Hz, 2H, 2-nphth). ES$^-$-MS for $\{C_{18}H_{13}N_4O_5\}^-$: calcd, 365.0879; obsd, 365.0886. Anal. Calcd for $C_{18}H_{13}N_4O_5K$: C, 53.46; H, 3.24; N, 13.85. Found: C, 53.71; H, 3.35; N, 14.08.

Potassium 2-[4-[(1,8-Naphthalamido)methyl]-1*H*-1,2,3-triazolyl]-acetate ($\mathbf{KL_{gly}}$). This compound was prepared via the same procedure as that for $\mathbf{KL_{ala}}$ using glycine (1.50 g, 20 mmol). Precipitation with 3 M HCl afforded 5.95 g (98% yield) of $\mathbf{HL_{gly}}$. This product (3.36 g, 10 mmol) was treated with 1 M methanolic KOH in the same manner as $\mathbf{HL_{ala}}$ to give $\mathbf{KL_{gly}}$ in quantitative yield (3.73 g, 10 mmol). ^{1}H NMR (CD_3OD): δ 4.92 (s, 2H, α-C*H*$_2$), 5.46 (s, 2H, C*H*$_2$), 7.81 (dd, J = 7.3 and 8.2 Hz, 2H, 3-nphth), 7.93 (s, 1H, triazole), 8.34 (dd, J = 0.9 and 8.4 Hz, 2H, 4-nphth), 8.58 (dd, J = 1.2 and 7.3 Hz, 2H, 2-nphth). ES$^-$-MS for $\{C_{17}H_{11}N_4O_4K\}^-$: calcd, 335.0794; obsd, 335.0780. Anal. Calcd for $C_{17}H_{11}N_4O_4K$: C, 54.54; H, 2.96; N, 14.96. Found: C, 54.76; H, 2.87; N, 15.09.

Preparation of Metal Complexes. Three solutions were prepared: a 5 mM aqueous solution of the metal acetate (Ni, Cu, Zn) or chloride (Fe, Co) (solution A), a mixture of 1:1 MeOH/H_2O (solution B), and a methanolic solution 10 mM in both $\mathbf{KL_{amino\ acid}}$ and 4,4′-bipyridine (solution C).

A 5 mL sample of solution A was placed in a 16 mm test tube, and 2 mL of B was carefully added to form a "buffer" layer. A 5 mL sample of C was layered on top, and the tube was tightly capped and left in a quiet location. Large hexagonal rods suitable for X-ray diffraction grew over a period of 10−15 days. For characterization and analysis, these insoluble crystals were washed several times with a 1:1 MeOH/H_2O solution to remove small amounts of noncrystalline impurities and then allowed to air-dry overnight.

Analytical figures were obtained for each complex containing the interstitial water molecules from crystals prepared in this manner (listed in the first line under each compound). Analytical figures for the dehydrated frameworks were measured by drying analytical samples of the corresponding hydrate to a constant weight (listed in the second line under each complex). In the case of both copper(II) complexes and the $[Fe(\mathbf{L_{ala}})_2(4,4'\text{-bipy})(H_2O)_2]\cdot 4.84H_2O$ complex, both the interstitial and coordinated water molecules were lost when the sample was dried to a constant weight.

$[Fe(\mathbf{L_{ala}})_2(4,4'\text{-bipy})(H_2O)_2]\cdot 4.84H_2O$. Anal. Calcd for $C_{46}H_{47.68}N_{10}O_{14.84}Fe$: C, 53.44; H, 4.65; N, 13.55. Found: C, 54.05; H, 4.52; N, 13.68.

Anal. Calcd for $C_{46}H_{34}N_{10}O_8Fe$: C, 60.67; H, 3.76; N, 15.38. Found: C, 60.43; H, 3.69; N, 15.33.

$[Co(\mathbf{L_{ala}})_2(4,4'\text{-bipy})(H_2O)_2]\cdot 4.76H_2O$. Anal. Calcd for $C_{46}H_{47.52}N_{10}O_{14.76}Co$: C, 53.35; H, 4.63; N, 13.53. Found: C, 54.08; H, 4.35; N, 13.55.

Anal. Calcd for $C_{46}H_{38}N_{10}O_{10}Co$: C, 58.17; H, 4.03; N, 14.75. Found: C, 57.89; H, 4.01; N, 14.62.

$[Ni(\mathbf{L_{ala}})_2(4,4'\text{-bipy})(H_2O)_2]\cdot 4.82H_2O$. Anal. Calcd for $C_{46}H_{46.5}N_{10}O_{14.82}Ni$: C, 53.59; H, 4.55; N, 13.59. Found: C, 53.80; H, 4.51; N, 13.65.

Anal. Calcd for $C_{46}H_{38}N_{10}O_{10}Ni$: C, 58.18; H, 4.03; N, 14.75. Found: C, 58.19; H, 3.87; N, 14.67.

$[Cu(\mathbf{L_{ala}})_2(4,4'\text{-bipy})(H_2O)_2]\cdot 4.25H_2O$. Anal. Calcd for $C_{46}H_{47.64}N_{10}O_{14.82}Ni$: C, 53.31; H, 4.63; N, 13.52. Found: C, 53.61; H, 4.35; N, 13.66.

Anal. Calcd for $C_{46}H_{34}N_{10}O_8Cu$: C, 60.16; H, 3.73; N, 15.25. Found: C, 59.76; H, 3.59; N, 15.08.

$[Cu(\mathbf{L_{ala}})_2(\mathbf{bipy})(H_2O)_2]\cdot 4.25D_2O$. Samples of $[Cu(L_{ala})_2(bipy)(H_2O)_2]\cdot 4.25D_2O$ were prepared by taking isolated crystals of $[Cu(L_{ala})_2(bipy)(H_2O)_2]\cdot 4.25H_2O$ and placing them inside a small vial with a perforated cap. This vial was placed inside a larger vial, and the contents were held under a vacuum for 24 h. D_2O (1 mL) was introduced into the space between the two vials. The system was then backfilled with dry nitrogen and allowed to rest undisturbed for 12 h.

Anal. Calcd for $C_{46}H_{38}D_{8.5}N_{10}O_{14.25}Cu$: C, 53.15; H + D, 5.33; N, 13.47. Found: C, 53.41; H + D, 5.08; N, 13.58.

$[Zn(\mathbf{L_{ala}})_2(4,4'\text{-bipy})(H_2O)_2]\cdot 4.74H_2O$. Anal. Calcd for $C_{46}H_{47.48}N_{10}O_{14.74}Zn$: C, 53.04; H, 4.59; N, 13.45. Found: C, 53.51; H, 4.20; N, 13.48.

Anal. Calcd for $C_{46}H_{38}N_{10}O_{10}Zn$: C, 57.78; H, 4.01; N, 14.65. Found: C, 57.75; H, 3.80; N, 14.63.

$[Co(\mathbf{L_{ser}})_2(4,4'\text{-bipy})(H_2O)_2]\cdot 4.68H_2O$. Anal. Calcd for $C_{46}H_{47.36}N_{10}O_{16.68}Co$: C, 51.82; H, 4.48; N, 13.14. Found: C, 52.19; H, 4.25; N, 13.08.

Anal. Calcd for $C_{46}H_{38}N_{10}O_{12}Co$: C, 56.27; H, 3.90; N, 14.27. Found: C, 56.03; H, 3.94; N, 13.97.

$[Ni(\mathbf{L_{ser}})_2(4,4'\text{-bipy})(H_2O)_2]\cdot 4.83H_2O$. Anal. Calcd for $C_{46}H_{47.66}N_{10}O_{16.83}Ni$: C, 51.70; H, 4.50; N, 13.11. Found: C, 52.51; H, 4.30; N, 13.04.

Anal. Calcd for $C_{46}H_{38}N_{10}O_{12}Ni$: C, 56.29; H, 3.90; N, 14.27. Found: C, 55.94; H, 4.00; N, 14.00.

$[Cu(\mathbf{L_{ser}})_2(4,4'\text{-bipy})(H_2O)_2]\cdot 4.35H_2O$. Anal. Calcd for $C_{46}H_{46.70}N_{10}O_{46.70}Cu$: C, 51.89; H, 4.42; N, 13.15. Found: C, 52.40; H, 3.97; N, 13.16.

Anal. Calcd for $C_{46}H_{34}N_{10}O_{10}Cu$: C, 58.13; H, 3.61; N, 14.74. Found: C, 57.93; H, 3.39; N, 14.73.

$[Zn(\mathbf{L_{ser}})_2(4,4'\text{-bipy})(H_2O)_2]\cdot 4.68H_2O$. Anal. Calcd for $C_{46}H_{47.36}N_{10}O_{16.68}Zn$: C, 51.51; H, 4.45; N, 13.06. Found: C, 51.87; H, 3.96; N, 13.11.

Anal. Calcd for $C_{46}H_{38}N_{10}O_{12}Zn$: C, 55.91; H, 3.88; N, 14.17. Found: C, 55.04; H, 3.67; N, 13.88.

$[Ni(\mathbf{L_{gly}})_2(4,4'\text{-bipy})(H_2O)_2]\cdot 5.52H_2O$. Anal. Calcd for $C_{44}H_{45.04}N_{10}O_{15.52}Ni$: C, 51.76; H, 4.45; N, 13.72. Found: C, 52.96; H, 4.38; N, 13.88.

Anal. Calcd for $C_{44}H_{34}N_{10}O_{10}Ni$: C, 57.35; H, 3.72; N, 15.20. Found: C, 57.13; H, 3.48; N, 15.03.

X-ray Crystallography. X-ray intensity data for most compounds were measured at 150(2) K using a Bruker SMART APEX diffractometer (Mo Kα radiation, λ = 0.710 73 Å), with a crystal-to-detector distance of 10.015 cm. For $[Fe(\mathbf{L_{ala}})_2(4,4'\text{-bipy})(H_2O)_2]\cdot 4.84H_2O$, the intensity data were measured at 295(2) K. Raw area detector data frame integration and correction for absorption effects were performed with the *SAINT*+ and *SADABS* programs.[31] Final unit cell parameters were determined by least-squares refinement of a large array of reflections from each data set. Direct method structure

(31) *SMART*, version 5.625; Bruker Analytical X-ray Systems, Inc.: Madison, WI, 2001. *SAINT*+, version 6.45; Bruker Analytical X-ray Systems, Inc.: Madison, WI, 2001.

solution, difference Fourier calculations, and full-matrix least-squares refinement against F^2 were performed with *SHELXTL*.[32]

The compounds are all isostructural. Systematic absences in the intensity data sets indicated one of the enantiomorphous space group pairs $P6_1/P6_5$ or $P6_122/P6_522$. The space group $P6_122$ or $P6_522$ was eventually confirmed by obtaining a good solution and refinement of the data and by evaluation of the absolute structure (Flack) parameter for each data set. For the hydrated structures, the asymmetric unit consists of (formally half of) one metal ion located on the C_2 rotational axis parallel to the [100] direction, one carboxylate ligand, half of a 4,4′-bipyridine ligand located on the same C_2 axis as the metal ion, a coordinated water molecule (O6), and a region of interstitial water molecules. The $-CH_2OH$ substituent of the $\mathbf{L_{ser}}$ ligand (C17 and O5) is disordered over two orientations. Counterpart bond distances of each disorder component were restrained to be similar; counterpart atoms were refined with identical displacement parameters. The total occupancy was constrained to sum to unity, and the major component occupancies for each compound were as follows: Co, 0.586(1); Cu, 0.555(4); Ni, 0.566; Zn, 0.605(4). Three interstitial water molecule sites were located: O1S, O2S, and O3S. O1S and O2S refined as fully occupied; O3S is located on the C_2 axis along the [1−20] direction and refined to less than full occupancy. The site occupancy and U_{iso} value for O3S were allowed to refine freely, resulting in physically reasonable values. The occupancies of O3S for each compound are given in Table 1. For $[Ni(\mathbf{L_{gly}})_2(4,4'\text{-bipy})(H_2O)_2]\cdot 5.52H_2O$, an additional water site, O4S, was refined. All non-hydrogen atoms were refined with anisotropic displacement parameters except O3S and O4S (isotropic). Hydrogen atoms bonded to carbon atoms were placed in geometrically idealized positions and included as riding atoms. The hydrogen atoms of the coordinated water O5 were located in difference maps and refined freely. Reasonable positions for the water hydrogen atoms of O1S and O2S were located in difference maps. After location, their coordinates were adjusted to $d(O-H) = 0.84$ Å and they were treated as riding on their parent oxygen atoms with $U(iso,H) = 1.5U(eq,O)$. No hydrogen atoms were located or calculated for O3S or O4S.

In the case of dehydrated crystals of $[Co(\mathbf{L_{ser}})_2(4,4'\text{-bipy})(H_2O)_2]$, initial refinement trials showed that the interstitial water content was either very low or nil. Refining a model with no interstitial water molecules gives R factors of R1/wR2 = 0.0655/0.1540 for $I > 2\sigma(I)$. A difference map calculated with this model gives a residual electron density peak maximum of 0.54 e/Å^3, located near C16; the second-largest peak is in the interstitial region with a magnitude of 0.49 e/Å^3. Assigning the second-largest peak as an oxygen atom of a water molecule and refining the occupancy and U_{iso} parameters freely give an occupancy value of 0.16(2) and $U_{iso} = 0.13(3)$ Å^2, translating to a water content of 0.32 interstitial H_2O per cobalt. The R factors decreased to R1/wR2 = 0.0640/0.1464 for $I > 2\sigma(I)$. There are other very weak peaks (0.30 e/Å^3) in the interstitial region, suggesting that the interstitial water was not completely removed under a vacuum.

Analyses of the structures were performed with the programs *TOPOS*[33] and *PLATON*.[34] Molecular surfaces were calculated using the MSMS library[35] within PMV,[36] and figures were rendered using POV-Ray.[37]

(32) *SHELXTL*, version 6.14; Bruker Analytical X-ray Systems, Inc.: Madison, WI, 2000.
(33) Blatov, V. A.; Shevchenko, A. P.; Serezhkin, V. N. *TOPOS*; Samara State University: Samara, Russia, 2000.
(34) Spek, A. L. *PLATON-97*; University of Utrecht: Utrecht, The Netherlands, 1997.
(35) Sanner, M. F.; Spehner, J.-C.; Olson, A. J. *Biopolymers* **1996**, *38*, 305–320.
(36) Sanner, M. F. *J. Mol. Graphics Modell.* **1999**, *17*, 57–61.
(37) Persistence of Vision Pty. Ltd. *Persistence of Vision (TM) Raytracer*; Persistence of Vision Pty. Ltd.: Williamstown, Victoria, Australia, 2004; http://www.povray.org/.

Results

Synthesis. The ligands were synthesized via a two-step, one-pot procedure using (for $K\mathbf{L_{ala}}$ and $K\mathbf{L_{ser}}$) L-amino acids (Chart 2). The amino acids are transformed into the corresponding azides by treatment with imidazole-1-sulfonyl azide hydrochloride in the presence of copper(II). The reaction of these azides with *N*-propargylnaphthalimide followed by precipitation with acid and treatment with base afforded the ligand $K\mathbf{L_{amino\ acid}}$.

Single crystals of 10 $[M(\mathbf{L_{amino\ acid}})_2(4,4'\text{-bipy})(H_2O)_2]\cdot 4xH_2O$ (M = Fe, Co, Ni, Cu, Zn; $x = 4.25$ to 5.52) complexes were grown via a layering method. An aqueous solution of an appropriate metal salt and a methanolic solution of 4,4′-bipyridine and $K\mathbf{L_{amino\ acid}}$, separated by a short "buffer" region of 1:1 methanol/water, were allowed to slowly diffuse into one another. Large hexagonal rods were observed for each metal/amino acid system after several days.

An attempt was also made to grow crystals of the copper and zinc complexes of $\mathbf{L_{ala}}^-$ under rigorously anhydrous conditions. In this case, a metal salt, 4,4′-bipyridine, and $K\mathbf{L_{ala}}$ were mixed in anhydrous methanol. A small amount of precipitate immediately formed, but no crystals or additional solid precipitate appeared, even over a period of several weeks. Upon the addition of water to this solution, the precipitate redissolved, and single crystals of $[M(\mathbf{L_{ala}})_2(4,4'\text{-bipy})(H_2O)_2]\cdot xH_2O$ grew over a period of several days.

Structural Analysis. Complexes containing the enantiopure ligands $\mathbf{L_{ala}}^-$ and $\mathbf{L_{ser}}^-$ based on L-amino acids crystallized in the space group $P6_122$, while those of the achiral ligand $\mathbf{L_{gly}}^-$ crystallized in the same tubes as two separate enantiomorphous crystals in the space groups $P6_122$ and $P6_522$. The asymmetric units of each metal complex for all ligands are isostructural, despite the changes in the amino acid side chain. In all of the complexes of $\mathbf{L_{ser}}^-$, the side chain $-CH_2OH$ group is disordered over two similar positions. Each structure has pockets containing 4.25−4.84 interstitial water molecules, where the amount varies slightly because the O3S position is only partially occupied.

In all of the complexes, the central metal ion is coordinated to two κ^1-carboxylate ligands, two water molecules, and one end each of two 4,4′-bipyridine ligands (Figure 1). In the cases of $\mathbf{L_{ala}}^-$ and $\mathbf{L_{ser}}^-$, the κ^1-carboxylate ligands are enantiopure and retain the stereochemistry of the L-amino acids from which they were formed. The metal ion is in an axially distorted octahedral environment, with each ligand type (carboxylate, water, bipyridine) coordinated in a trans arrangement. One hydrogen atom on each of the coordinated water molecules makes an intramolecular hydrogen bond to each of the noncoordinated oxygen atoms of the carboxylate ligands. The amount of octahedral distortion varies with the identity of each metal ion, with the most distorted environments found in the copper(II) complexes (ca. 0.3 Å longer bonds to the coordinated waters), as expected for this metal ion with a well-known large Jahn−Teller distortion.[38] In contrast, the zinc(II) complex exhibits little distortion, as determined by comparing

(38) (a) Noro, S. *Phys. Chem. Chem. Phys.* **2010**, *12*, 2519–2531. (b) Bersuker, I. *J. Mol. Struct.* **2007**, *838*, 44–52. (c) Zhang, J.; Chen, X. *J. Am. Chem. Soc.* **2009**, *131*, 5516–5521. (d) Horike, S.; Shimomura, S.; Kitagawa, S. *Nat. Chem.* **2009**, *1*, 695–704. (e) Fletcher, A.; Thomas, K.; Rosseinsky, M. *J. Solid State Chem.* **2005**, *178*, 2491–2510. (f) Bradshaw, D.; Claridge, J. B.; Cussen, E. J.; Prior, T. J.; Rosseinsky, M. J. *Acc. Chem. Res.* **2005**, *38*, 273–282.

Table 1. Selected Crystallographic and Refinement Data

	[Fe($\mathbf{L_{ala}}$)$_2$-(4,4′-bipy)(H$_2$O)$_2$]·4.84H$_2$O	[Co($\mathbf{L_{ala}}$)$_2$-(4,4′-bipy)(H$_2$O)$_2$]·4.76H$_2$O	[Ni($\mathbf{L_{ala}}$)$_2$-(4,4′-bipy)(H$_2$O)$_2$]·4.82H$_2$O	[Cu($\mathbf{L_{ala}}$)$_2$-(4,4′-bipy)(H$_2$O)$_2$]·4.25H$_2$O
color	brick orange	pink orange	green	dark green
formula	$C_{46}H_{47.68}N_{10}O_{14.84}Fe$	$C_{46}H_{47.52}N_{10}O_{14.76}Co$	$C_{46}H_{47.64}N_{10}O_{14.82}Ni$	$C_{46}H_{46.50}N_{10}O_{14.25}Cu$
O3S occupancy	0.84(2)	0.77(2)	0.82(2)	0.25
space group	$P6_122$	$P6_122$	$P6_122$	$P6_122$
a (Å)	11.4707(3)	11.3686(1)	11.2927(1)	11.2004(3)
c (Å)	61.655(3)	61.4475(11)	61.771(1)	62.448(3)
volume (Å^3)	7025.6(5)	6877.79(15)	6821.98(14)	6784.4(4)
Z	6	6	6	6
size (mm^3)	0.30 × 0.28 × 0.24	0.48 × 0.38 × 0.16	0.40 × 0.38 × 0.35	0.28 × 0.10 × 0.08
no. of reflns	86 138	44 445	25 722	73 059
no. of indep reflns	4164	4078	4046	4015
no. of param	333	335	335	326
GOF	1.171	1.159	1.116	1.042
Flack param	0.06(3)	0.02(2)	0.02(2)	0.016(17)
final R1 [$I > 2\sigma(I)$]	0.0543	0.0459	0.0460	0.0411
wR2 (all data)	0.1262	0.1101	0.1081	0.0914

	[Cu($\mathbf{L_{ala}}$)$_2$-(4,4′-bipy)(H$_2$O)$_2$]	[Zn($\mathbf{L_{ala}}$)$_2$-(4,4′-bipy)(H$_2$O)$_2$]·4.74H$_2$O	[Co($\mathbf{L_{ser}}$)$_2$-(4,4′-bipy)(H$_2$O)$_2$]·4.68H$_2$O	[Co($\mathbf{L_{ser}}$)$_2$-(4,4′-bipy)(H$_2$O)$_2$]·0.32H$_2$O
color	dark blue	yellow	pink orange	pink orange
formula	$C_{46}H_{38}N_{10}O_{10}Cu$	$C_{46}H_{47.48}N_{10}O_{14.74}Zn$	$C_{46}H_{47.36}N_{10}O_{16.68}Co$	$C_{46}H_{38.64}N_{10}O_{12.32}Co$
O3S occupancy	0	0.74(2)	0.68(1)	0.16(2) (O1S)
space group	$P6_122$	$P6_122$	$P6_122$	$P6_122$
a (Å)	11.1347(3)	11.3650(1)	11.3835(2)	11.4398(4)
c (Å)	60.938(3)	61.510(1)	61.2732(15)	58.718(5)
volume (Å^3)	6543.0(4)	6880.42(14)	6876.3(2)	6654.8(6)
Z	6	6	6	6
size (mm^3)	0.36 × 0.12 × 0.10	0.40 × 0.35 × 0.32	0.38 × 0.36 × 0.22	0.34 × 0.28 × 0.26
no. of reflns	93818	60898	43451	43817
no. of indep reflns	3858	5303	4720	3535
no. of param	306	335	350	327
GOF	1.256	1.136	1.115	1.284
Flack param	0.04(2)	0.023(13)	0.010(15)	0.08(4)
final R1 [$I > 2\sigma(I)$]	0.0558	0.0443	0.0378	0.0640
wR2 (all data)	0.1279	0.1076	0.0886	0.1464

	[Ni($\mathbf{L_{ser}}$)$_2$-(4,4′-bipy)(H$_2$O)$_2$]·4.83H$_2$O	[Cu($\mathbf{L_{ser}}$)$_2$-(4,4′-bipy)(H$_2$O)$_2$]·4.35H$_2$O	[Zn($\mathbf{L_{ser}}$)$_2$-(4,4′-bipy)(H$_2$O)$_2$]·4.68H$_2$O	[Ni($\mathbf{L_{gly}}$)$_2$-(4,4′-bipy)(H$_2$O)$_2$]·5.52H$_2$O
color	green	dark green	yellow	green
formula	$C_{46}H_{47.66}N_{10}O_{16.83}Ni$	$C_{46}H_{46.71}N_{10}O_{16.35}Cu$	$C_{46}H_{47.36}N_{10}O_{16.68}Zn$	$C_{44}H_{45.04}N_{10}O_{15.52}Ni$
O3S occupancy	0.83(2)	0.35(2)	0.68(1)	1.52(2) (O3S + O4S)
space group	$P6_122$	$P6_122$	$P6_122$	$P6_522$
a (Å)	11.3480(4)	11.2179(1)	11.3689(2)	11.3315(2)
c (Å)	62.182(3)	62.4758(12)	61.3502(16)	59.8555(16)
volume (Å^3)	6934.8(5)	6808.72(16)	6867.3(2)	6655.9(2)
Z	6	6	6	6
size (mm^3)	0.26 × 0.24 × 0.20	0.38 × 0.32 × 0.18	0.42 × 0.22 × 0.18	0.38 × 0.36 × 0.20
no. of reflns	100 071	36 980	53 609	36 302
no. of indep reflns	4779	4636	4706	4222
no. of param	350	350	350	329
GOF	1.221	1.165	1.224	1.058
Flack param	0.011(17)	0.026(15)	0.023(13)	0.00(2)
final R1 [$I > 2\sigma(I)$]	0.0406	0.0405	0.0373	0.0534
wR2 (all data)	0.1032	0.0978	0.0902	0.1296

the $H_2O-M-OH_2$ and $COO-M-OOC$ bond distances and angles; selected parameters for each compound are given in Table 2.

The dominant structural feature for all of these complexes is the organization of the individual metallic units into a large helix, held together *solely* by strong, noncovalent $\pi\cdots\pi$ stacking interactions of the 1,8-naphthalimide groups, indicated for [Zn($\mathbf{L_{ala}}$)$_2$(4,4′-bipy)(H$_2$O)$_2$]·4.74H$_2$O in Figure 2 by the arrows and circles. Each naphthalimide group of the basically linear divalent metal units shown in Figure 1 interacts with a second naphthalimide group, forming the helix, with the repeat unit containing six divalent metal complexes. The helices are extremely large; one turn of the helix travels ∼60 Å (the length of the crystallographic *c* axis) and has a diameter of ca. 40 Å. This arrangement of the divalent metallic units orients the polymeric chains formed by the 4,4′-bipyridine ligands perpendicular to the helix, rotating the chains by 60° as one moves along the helix from one metallic unit to the next.

A key issue to the formation of the helical arrangement is the relative orientation of each naphthalimide ring pair in the $\pi\cdots\pi$ stacking interactions. In many of the structures that

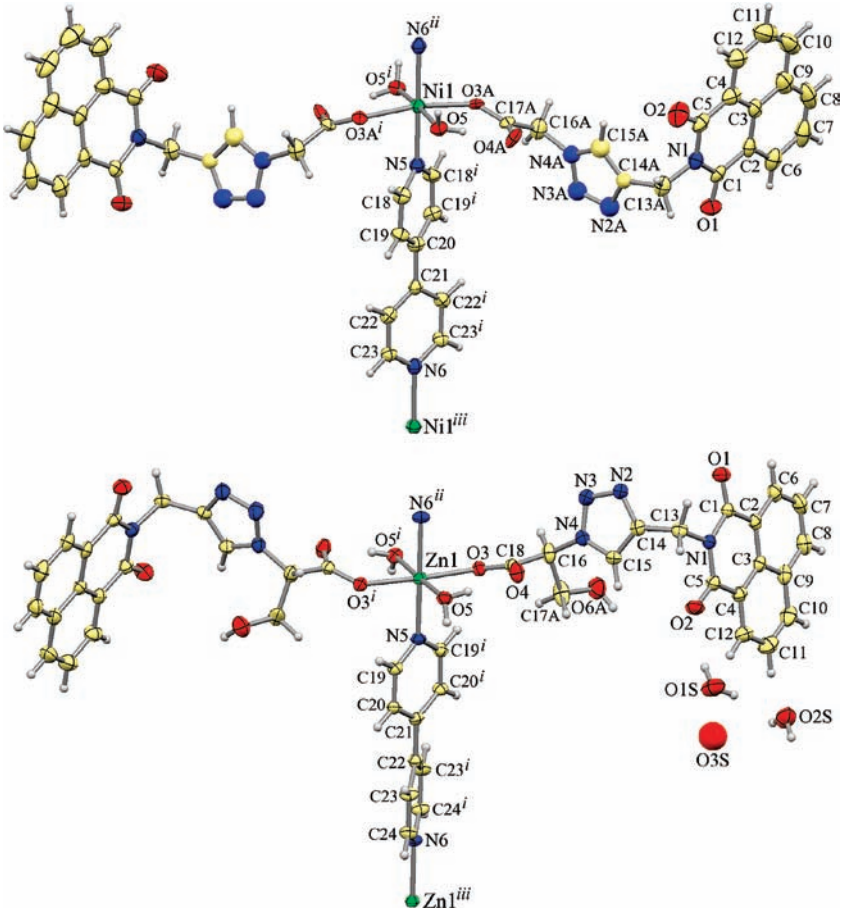

Figure 1. Representative repeating unit, from $[Ni(\mathbf{L_{gly}})_2(4,4'\text{-bipy})(H_2O)_2]\cdot 5.52H_2O$ (top, from the *M* helix) and $[Zn(\mathbf{L_{ser}})_2(4,4'\text{-bipy})(H_2O)_2]\cdot 4.68H_2O$, disorder component A (bottom). The numbering schemes for complexes of $\mathbf{L_{ala}}$ and $\mathbf{L_{ser}}$ are identical, with the exception of O6.

Chart 2. Synthesis of the $K\mathbf{L_{amino\ acid}}$ Ligands [R = H ($K\mathbf{L_{gly}}$), CH_3 ($K\mathbf{L_{ala}}$), CH_2OH ($K\mathbf{L_{ser}}$)]

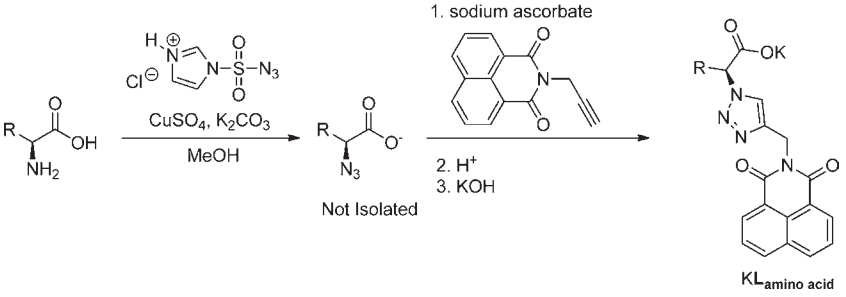

Table 2. Selected Bond Distances and Angles

ligand	metal	M−OH_2 (Å)	H_2O−M−OH_2 (deg)	COO−M (Å)	COO−M−OOC (deg)	N−M (Å)
$\mathbf{L_{ala}}$	Fe	2.15	177	2.10	178	2.18
	Co	2.10	178	2.09	177	2.14
	Ni	2.06	178	2.07	177	2.09
	Cu	2.34	179	2.01	177	2.04
	Zn	2.12	179	2.11	177	2.14
$\mathbf{L_{ser}}$	Co	2.11	177	2.09	177	2.14
	Ni	2.08	178	2.06	177	2.12
	Cu	2.40	178	1.98	179	2.05
	Zn	2.12	178	2.12	177	2.14
$\mathbf{L_{gly}}$	Ni	2.07	175	2.07	175	2.11

we have reported previously, the 1,8-naphthalimide groups are arranged with the dipole vectors of this group (running through the central ring carbon atoms, pointing toward the nitrogen) oriented at 180° (head-to-tail arrangement), although we have shown that skewed arrangements are observed in many cases and that this rotation does not significantly affect the energy of the interaction.[22] In the structures reported here, the dipole vectors are highly skewed,

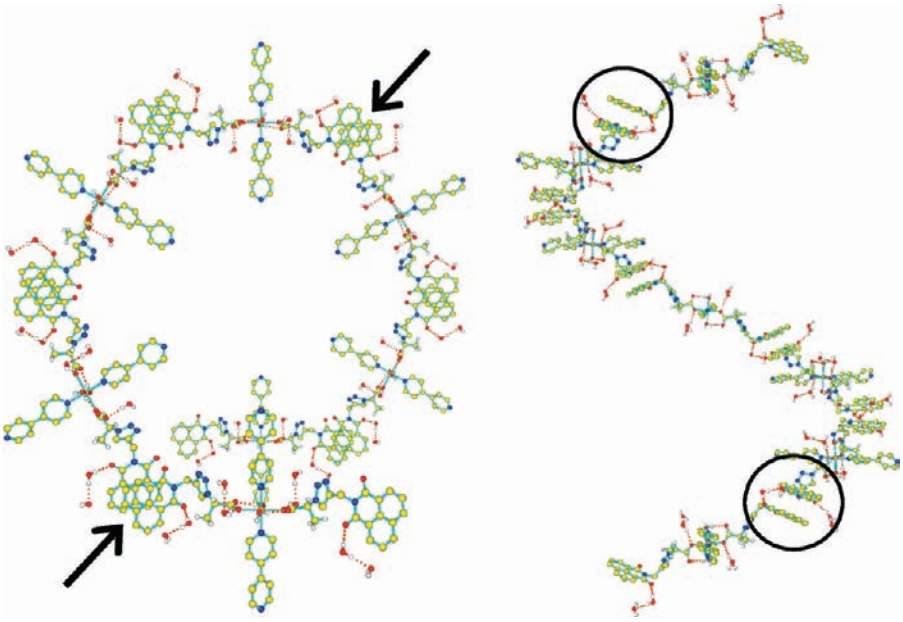

Figure 2. π-Stacked *P* helix of $[Zn(\mathbf{L_{ala}})_2(4,4'\text{-bipy})(H_2O)_2]\cdot 4.74H_2O$, showing the fully occupied interstitial water pairs: (left) view down the helix axis; (right) view perpendicular to the helix axis. The arrows and circles locate two of the strong, noncovalent, $\pi\cdots\pi$ stacking interactions between naphthalimide groups.

Table 3. Parameters for $\pi\cdots\pi$ Stacking Interactions

ligand	metal	dipole angle (deg)	plane−plane angle (deg)	plane−plane distance (Å)	χ (Å)
$\mathbf{L_{ala}}^-$	Fe	68	6.5	3.48	0.70
	Co	67	7.2	3.45	0.61
	Ni	66	6.9	3.44	0.53
	Cu	66	5.5	3.42	0.43
	Zn	67	6.8	3.44	0.60
$\mathbf{L_{ser}}^-$	Co	65	4.9	3.42	0.62
	Ni	64	6.3	3.43	0.66
	Cu	65	4.0	3.40	0.44
	Zn	65	4.9	3.43	0.60
$\mathbf{L_{gly}}^-$	Ni	68	5.9	3.42	0.76

oriented in the range 64−68° (Table 3). It is this orientation that mainly supports the formation of a helical structure, even though it is built by trans-coordinated carboxylate ligands that adopt a nearly linear conformation.

Despite the inclusion of a different side chain (CH_2OH instead of CH_3) that is both bulkier and has the option of forming additional hydrogen bonds, complexes of $\mathbf{L_{ala}}^-$ and $\mathbf{L_{ser}}^-$ are isostructural; the same helical structure forms, with a *P* orientation, supported by the $\pi\cdots\pi$ stacking interactions (Figure 3) with very similar structural properties (Tables 2 and 3). The amino acid side chains adopt extremely similar configurations, as indicated by the similarity of the helices in the figure.

The nickel(II) complex of the achiral ligand $\mathbf{L_{gly}}^-$, $[Ni(\mathbf{L_{gly}})_2(4,4'\text{-bipy})(H_2O)_2]\cdot 4.52H_2O$, has also been characterized crystallographically. Crystallization of this complex produces two types of homochiral crystals in the same tube, one in the enantiomorphous space groups $P6_122$ and the other in $P6_522$, a clear example of *spontaneous resolution*.[39] Helices in the crystals formed in the space group $P6_122$ adopt a right-handed (*P*) conformation, analogous to the complexes reported above, while those in the space group $P6_522$ adopt the left-handed (*M*) conformation, both of which are shown in Figure 4. Aside from a lack of a chiral preference, the overall structure of the $\mathbf{L_{gly}}^-$ complex is very similar to those of complexes $\mathbf{L_{ala}}^-$ and $\mathbf{L_{ser}}^-$.

The $\pi\cdots\pi$ stacking parameters of the 1,8-naphthalimide groups indicate that the rings are properly oriented for substantial interactions in all of the structures. There are three main parameters to consider when characterizing the strength of the $\pi\cdots\pi$ stacking interaction: the distance from the plane of one ring to another, the angle between the rings, and the amount of surface area that overlaps, described by the amount that the rings are "slipped" relative to one another. While the first two parameters are well established (the plane−plane distances reported here are the average of the length of the vector normal to each plane, originating from the two central ring carbon atoms),[15a] the "slippage" parameter, χ, has recently been defined to indicate the amount that the two naphthalimide rings are offset from one another.[22] The value is the third side of the right triangle (red line) formed with the average perpendicular distance (green line) between the rings and the line joining the central fused ring carbon atoms (C3−C3 in this case, blue line) of the two rings, illustrated in Figure 5. Parameters related to the $\pi\cdots\pi$ stacking interactions are summarized in Table 3.

As indicated above, neighboring helices are connected through the bipyridine chains that run perpendicularly to them; the orientation of the bipyridine chains is determined by the 6-fold screw axis of the helix. Figure 6 shows two different representations of a segment of the structure containing seven helices; both a cartoon representation (left) and a standard representation (right) are shown, with the same perspective. One layer of the structure is indicated by a box. The bipyridine chains, shown abbreviated as magenta cylinders, are terminated by arrows that indicate their "direction". Ligands sharing a common bipyridine axis in each layer share matching colors. Because of the rotation of the bipyridine axes along the *c* axis of the crystal, this one-dimensional interaction supports two of the three dimensions of the structure.

(39) (a) Morris, R.; Bu, X. *Nat. Chem.* **2010**, *2*, 353–361. (b) Perez-Garcia, L.; Amabilino, D. *Chem. Soc. Rev.* **2002**, *31*, 342–356.

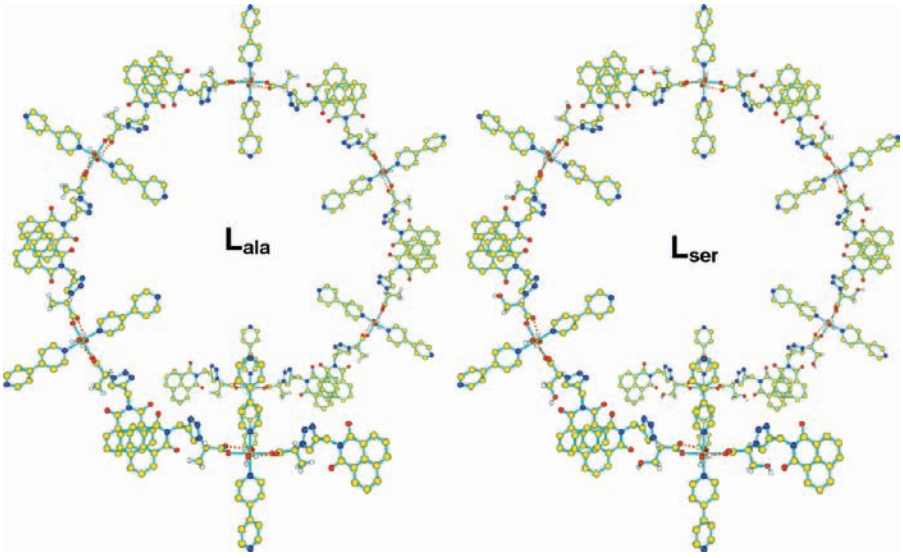

Figure 3. Comparison of the π-stacked *P* helices of $[Zn(\mathbf{L_{ala}})_2(4,4'\text{-bipy})(H_2O)_2]\cdot 4.74H_2O$ (left) and $[Zn(\mathbf{L_{ser}})_2(4,4'\text{-bipy})(H_2O)_2]\cdot 4.68H_2O$. Only the major disorder component of the $-CH_2OH$ side chain is shown. Both helices are viewed down the helical axis.

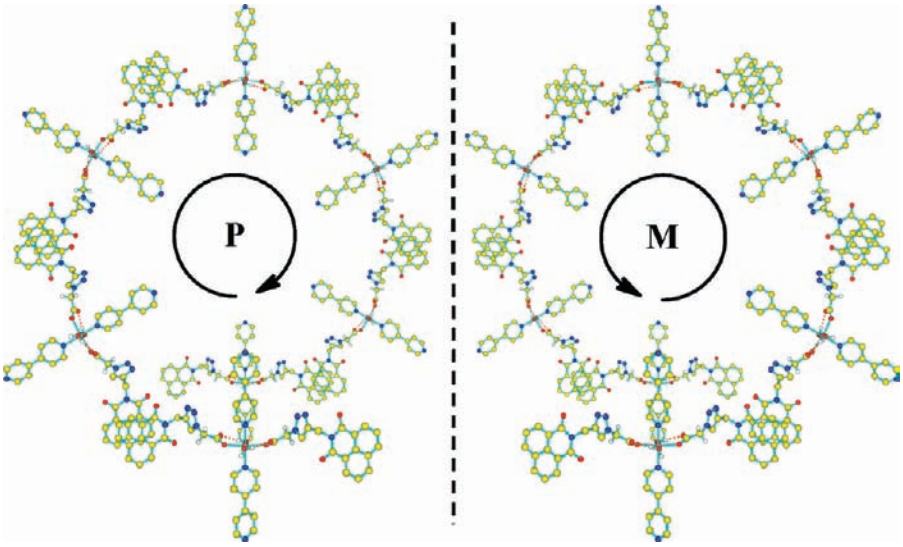

Figure 4. Comparison between enantiomorphous helices formed by $[Ni(\mathbf{L_{gly}})_2(4,4'\text{-bipy})(H_2O)_2]\cdot 5.52H_2O$. Helices from both $P6_122$ (on the left) and $P6_522$ (on the right) crystals are shown.

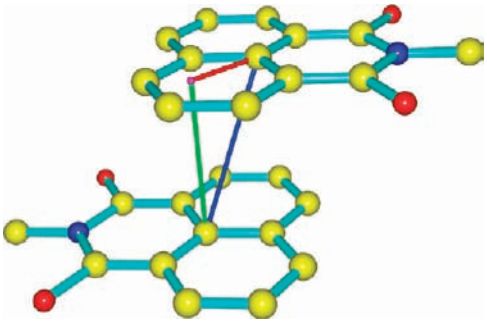

Figure 5. Schematic illustration of the slippage parameter, χ, the length of the red line.

Each layer of the helix (as indicated by the box in Figure 6) is also supported by additional supramolecular interactions. The hydrogen atoms of the coordinated water molecules not involved in the intramolecular hydrogen bond to the carboxylate ligands form hydrogen bonds with naphthalimide carbonyl oxygen atoms from two different adjacent bipyridine chains, as shown by dashed magenta lines in Figure 7. This sheet is further supported by $\pi\cdots\pi$ stacking of the bipyridine rings with naphthalimide groups of neighboring chains (closest atom−atom contact = 3.504 Å). These interactions can be best seen in the center of Figure 7, which shows the central layer from Figure 6, viewed down the helical axis. The green bipyridine groups are sandwiched between dark-blue naphthalimide rings (above) and red naphthalimide rings (below).

The overall effect of these interactions affords a tightly interconnected structure, where the helices formed by the $\pi\cdots\pi$ stacking interactions are nestled closely against each other. A representation of the sum of these interactions, which also shows the pockets holding the interstitial water molecules, is shown in Figure 8.

The noncoordinated, interstitial water molecules are held inside the framework of the $\mathbf{L_{ala}}^-$ complexes by

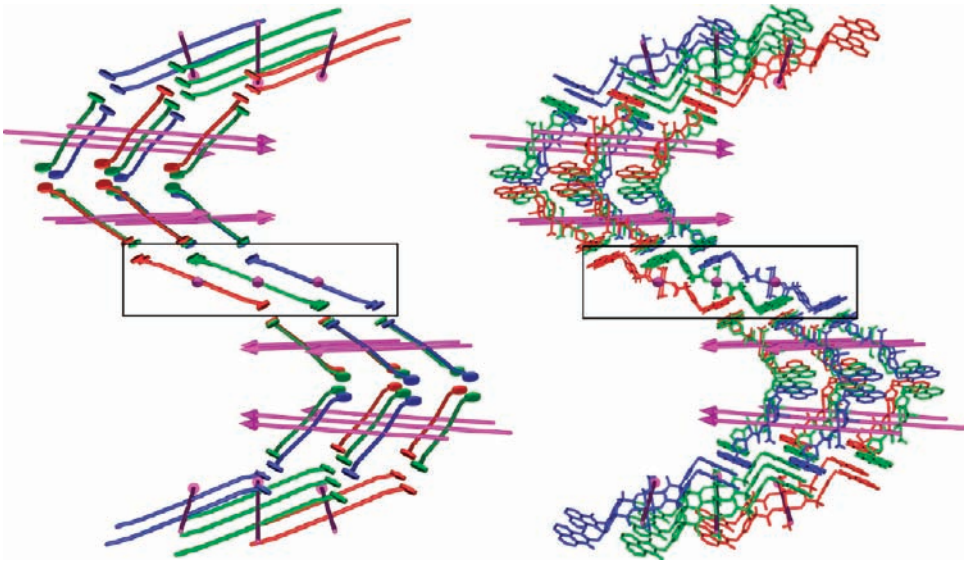

Figure 6. Left: Cartoon representation of adjacent $\pi\cdots\pi$-stacked helices for $[Cu(\mathbf{L_{ala}})_2(4,4'\text{-bipy})(H_2O)_2]\cdot 4.25H_2O$. The red, green, and blue colors indicate repeating units sharing a common bipyridine axis (magenta arrows). Right: Standard representation. The boxes indicate one "layer" of the helix.

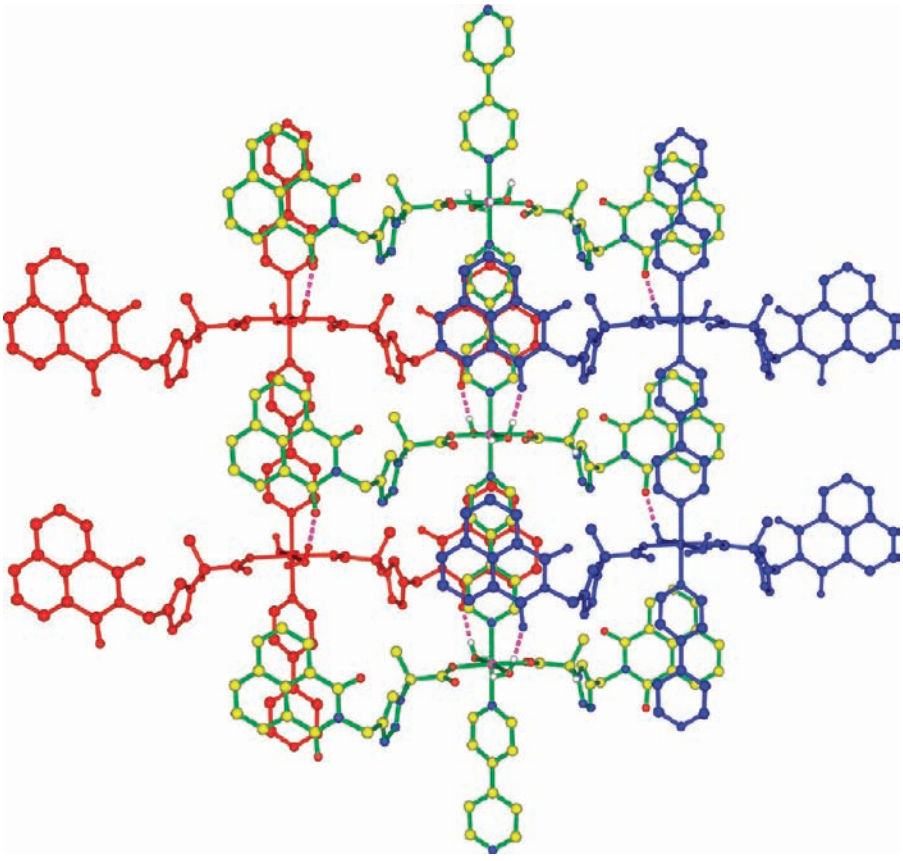

Figure 7. Perpendicular view of a single sheet of $[Cu(\mathbf{L_{ala}})_2(4,4'\text{-bipy})(H_2O)_2]\cdot 4.25H_2O$, down the crystallographic *c* axis. Interchain hydrogen bonds are indicated by dashed magenta lines.

hydrogen-bonding interactions. Two water molecules that are hydrogen-bonded (O1S and O2S) to each other link one naphthalimide carbonyl oxygen (O2) with the metal-coordinated oxygen of a carboxylate ligand (O3) on an adjacent helix with additional hydrogen bonds. This pair of water molecules is weakly hydrogen-bonded via the partially occupied third interstitial water molecule, O3S, to an identical symmetry-related pair (O1S′ and O2S′); this symmetry related pair links two different helices than does the first pair (Figure 9).

While the hydrogen atoms participating in the interstitial water hydrogen-bonding network in the $\mathbf{L_{gly}}^-$ framework could not be located, the positions of and distances between the oxygen atoms (O1S, O2S, and O3S) are similar to those found for the complexes of $\mathbf{L_{ala}}^-$, suggesting that the hydrogen-bonding network is the

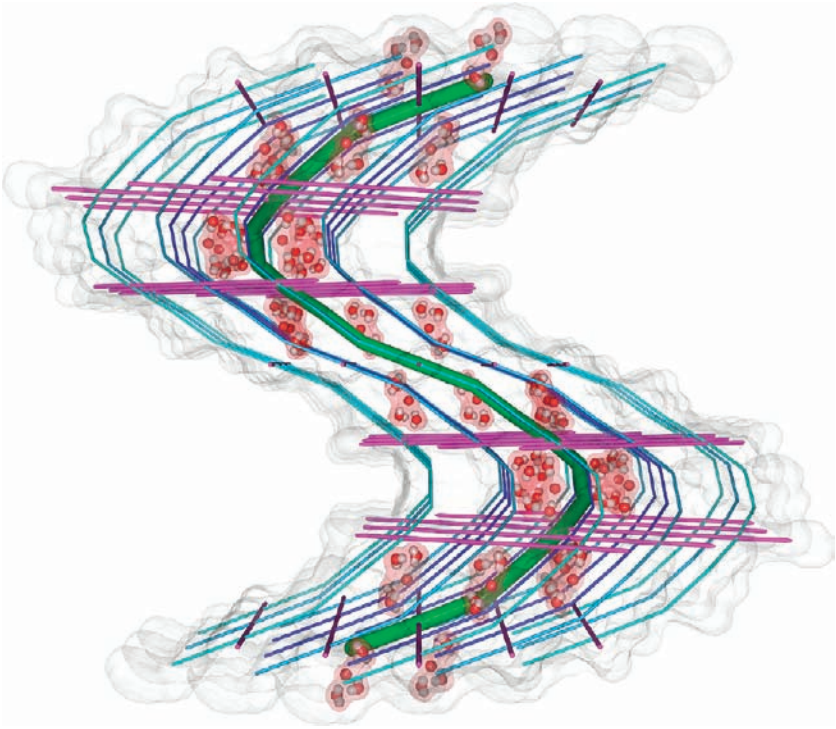

Figure 8. Representation of a large segment of the structure for $[Cu(\mathbf{L_{ala}})_2(4,4'\text{-bipy})(H_2O)_2]\cdot 4.25H_2O$. The central helix (green cylinder) is shown linked to its neighbors (blue cylinders) by the bipyridine groups (magenta cylinders); the red areas show the isolated pockets of interstitial water molecules. The molecular surface of both the helices (gray shadows) and pockets of water (red shadows) is also shown.

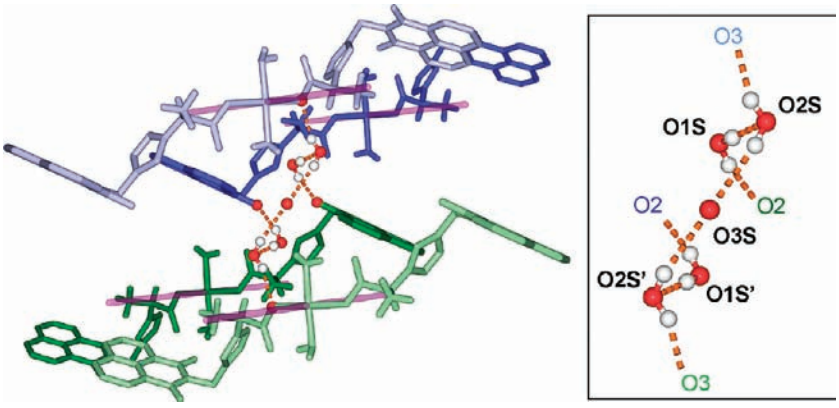

Figure 9. Hydrogen-bonding network in $[Zn(\mathbf{L_{ala}})_2(4,4'\text{-bipy})(H_2O)_2]\cdot 4.74H_2O$. The colors of the ligands (blue and green) indicate that they are in the same layer. The bipyridine ligands are shown as magenta cylinders.

same. Similarly, the inclusion of additional steric bulk and hydrogen-bonding functionality in the complexes of $\mathbf{L_{ser}}^-$ has very little effect on the overall structure of the interstitial water molecules. The sole difference, seen in Figure 10, arises from the hydroxyl group present in the serine side chain, which hydrogen bonds to the interstitial water molecules through O1S, causing each pair of water molecules to now link three helices; the other hydrogen bonds formed by the interstitial water molecules are the same as those described above for the alanine- and glycine-based complexes.

A summary of the relevant parameters in the hydrogen-bonding interactions for each of the frameworks is presented in Table 4. The values shown are averages for each interaction in all of the structures, with the exception of the "side chain−chain" interaction, which only occurs in complexes of $\mathbf{L_{ser}}^-$.

As shown in Figure 11, the interstitial water molecules hydrogen bonded to one helix (red) are involved in hydrogen-bonding interactions with six neighboring helices (solid colors). An additional six helices (transparent colors) are connected to the others by the bipyridine axis; they do not directly interact with the interstitial water pairs but form the "walls" of the areas in which the pairs reside. As shown in Figures 8 and 11, there are no void spaces or channels in these structures other than the pockets holding the interstitial water molecules, pockets clearly isolated from each other.

Single-Crystal to Single-Crystal Transformations. Placing crystals of $[Cu(\mathbf{L_{ala}})_2(4,4'\text{-bipy})(H_2O)_2]\cdot 4.25H_2O$ under a vacuum for several hours leads to a dramatic green to blue color change with no loss of crystallinity (Figure 12). Reintroduction of water vapor to the dehydrated crystals by a few hours of exposure to atmospheric

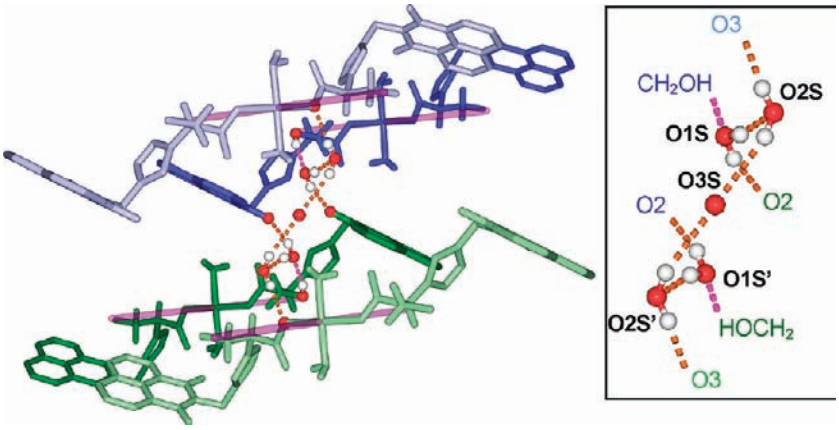

Figure 10. Hydrogen-bonding network in the $[Zn(\mathbf{L}_{ser})_2(4,4'\text{-bipy})(H_2O)_2]\cdot 4.68H_2O$ system. Orange dashed lines indicate hydrogen bonds isostructural with those in the $[M(\mathbf{L}_{ala})_2(4,4'\text{-bipy})(H_2O)_2]\cdot xH_2O$ complexes, whereas the magenta dashed lines indicate the side chain $OH\cdots H_2O$ hydrogen bonds. Only the major disorder component of the $-CH_2OH$ side chain is shown.

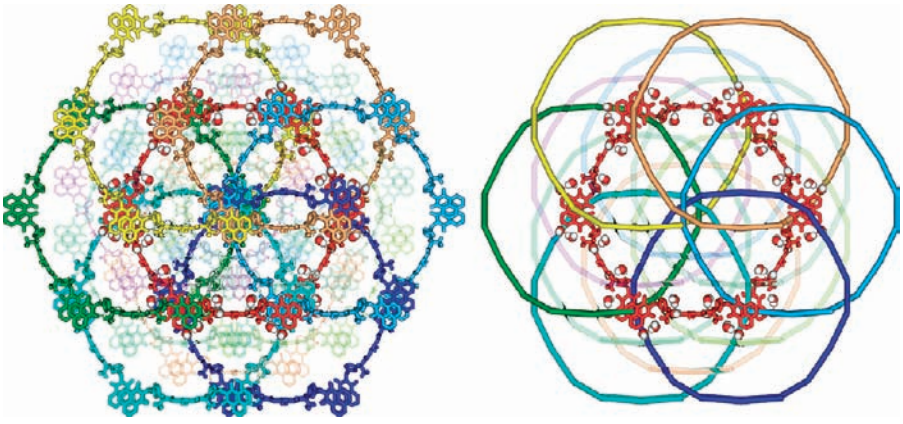

Figure 11. Left: Helices interconnected by the hydrogen-bonded pairs of interstitial water molecules. The central (red) helix interacts with each of the six exterior colored helices through hydrogen-bonding water molecules. Neighboring helices interacting only through bipyridine chains (omitted) are shown as transparent. Right: Simplified representation.

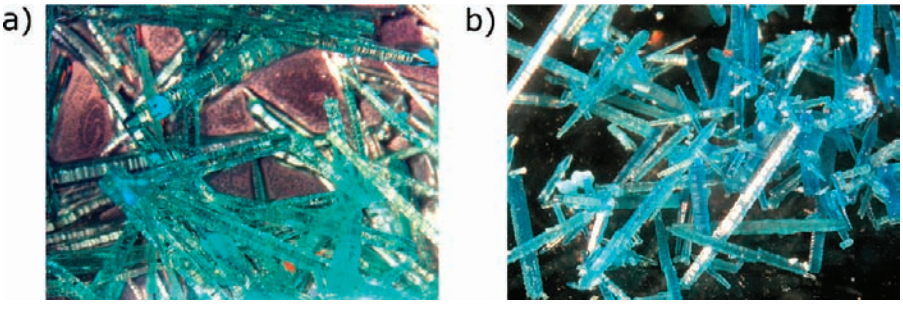

Figure 12. Crystals of $[Cu(\mathbf{L}_{ala})_2(4,4'\text{-bipy})(H_2O)_2]\cdot 4.25H_2O$ (a) before and (b) after dehydration.

Table 4. Average Interaction Distances and Angles, in Å and deg, in the Hydrogen-Bonded Interstitial Water Molecules

type	donor	hydrogen	acceptor	D−H	H···A	D···A	D−H···A
nphth−water	O1S	H1SA	O2	0.84	2.09	2.90	163
acid−water	O2S	H2SB	O3	0.84	2.12	2.92	162
strong water−water	O1S	H1SB	O2S	0.84	1.96	2.79	168
weak water−water	O2S	H2SA	O3S	0.84	2.42	3.24	164
side chain−water[a]	O5B	H5B	O1S	0.84	1.97	2.78	165

[a] This interaction is only present in the $\mathbf{L}_{ser}^-$ frameworks. Values are for the major disorder component of the $-CH_2OH$ side chain.

moisture leads to a blue to green color change, indicating reversal of the process. The crystals maintain their integrity during this process. X-ray crystallographic studies of the initial, dehydrated, and rehydrated forms definitively demonstrate that the color change is caused by removal and reintroduction of the interstitial water molecules. There is no change in the coordination sphere of the metal ion; the two water ligands coordinated to the copper(II) are not

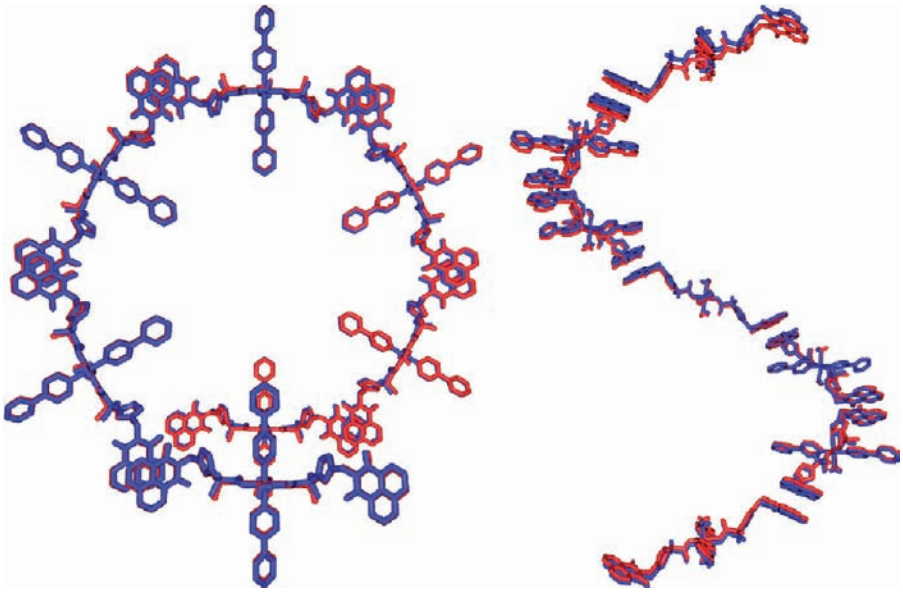

Figure 13. Comparison of the helices formed by $[Cu(\mathbf{L_{ala}})_2(4,4'\text{-bipy})(H_2O)_2]\cdot 4.25H_2O$ (blue) and $[Cu(\mathbf{L_{ala}})_2(4,4'\text{-bipy})(H_2O)_2]$ (red): (left) view down the helix axis; (right) view perpendicular to the helix axis.

removed. This process is a *dramatic* example of a single-crystal to single-crystal transformation.

After removal of the interstitial water, the major features of the solid-state structures remain largely unaffected. The largest difference observed is in the geometry of the hydrogen bond from the coordinated water molecules to the naphthalimide carbonyl oxygen atoms shown in Figure 7. Upon dehydration, the O−H···O angle changes from 177° to 153°. A unit cell contraction is also observed. The volume of the cell decreases by 3.7%; the largest contraction occurs along the *c* axis, which corresponds to the helical axis. Superimposing helices from a hydrated and dehydrated crystal (see Figure 13) illustrates the minor differences in the conformation of the ligands, as well as contraction of the *c* axis.

While calculations carried out with PLATON show no additional solvent-accessible void space in the hydrated form, calculations on the dehydrated form show that the space formerly occupied by the interstitial water molecules is now void space. The void space occupies 530 $Å^3$ per unit cell, which is 8.1% of the total unit cell volume. This space is slightly smaller than the amount of space occupied by the interstitial water in the hydrated structure, which was calculated to be 696 $Å^3$ per unit cell (10.3% of the total hydrated unit cell volume).

The hydration−dehydration process was fully reversible, even when H_2O was replaced by D_2O. Dehydration of $[Cu(\mathbf{L_{ala}})_2(4,4'\text{-bipy})(H_2O)_2]\cdot 4.25H_2O$ and "rehydration" with D_2O can be followed by IR spectroscopy. The broad O−H stretching band centered at 3462 cm^{-1} in $[Cu(\mathbf{L_{ala}})_2(4,4'\text{-bipy})(H_2O)_2]\cdot 4.25H_2O$ disappears upon dehydration and reappears at 2576 cm^{-1} after exposure to D_2O vapor (Figure 14). To rule out the possibility that these spectral changes arise from a surface adsorption of D_2O, elemental analysis on the crystals formed in "rehydration" with D_2O show that the formula $[Cu(\mathbf{L_{ala}})_2(4,4'\text{-bipy})(H_2O)_2]\cdot 4.25D_2O$ is correct. The sharper band at 3555 cm^{-1} in dehydrated $[Cu(\mathbf{L_{ala}})_2(4,4'\text{-bipy})(H_2O)_2]$ and $[Cu(\mathbf{L_{ala}})_2(4,4'\text{-bipy})(H_2O)_2]\cdot 4.25D_2O$ (obscured by the broad 3462 cm^{-1} in $[Cu(\mathbf{L_{ala}})_2(4,4'\text{-bipy})(H_2O)_2]\cdot 4.25H_2O$) is assigned to the metal-coordinated water molecules.

The relatively low-quality crystals of the serine ligand analogue, $[Cu(\mathbf{L_{ser}})_2(4,4'\text{-bipy})(H_2O)_2]\cdot 4.35H_2O$, exhibit the same color change when placed under a vacuum but degrade to the point where they are unsuitable for high-quality, single-crystal X-ray structural analysis. In contrast, the analogous cobalt complex, $[Co(\mathbf{L_{ser}})_2(4,4'\text{-bipy})(H_2O)_2]\cdot 4.68H_2O$, forms higher quality crystals; therefore, crystals of $[Co(\mathbf{L_{ser}})_2(4,4'\text{-bipy})(H_2O)_2]\cdot 4.68H_2O$ were used for the dehydration studies. After being held under a vacuum for several days, X-ray crystallography confirmed the structure as the dehydrated complex $[Co(\mathbf{L_{ser}})_2(4,4'\text{-bipy})(H_2O)_2]$. There is a contraction of the unit cell (the largest being a 4.2% reduction along the *c* axis), similar to that observed for $[Cu(\mathbf{L_{ala}})_2(4,4'\text{-bipy})(H_2O)_2]\cdot 4.25H_2O$. Again, reintroduction of water vapor to a crystal of $[Co(\mathbf{L_{ser}})_2(4,4'\text{-bipy})(H_2O)_2]$ leads to the re-formation of $Co(\mathbf{L_{ser}})_2(4,4'\text{-bipy})(H_2O)_2]\cdot 4.68H_2O$. The void volume in $[Co(\mathbf{L_{ser}})_2(4,4'\text{-bipy})(H_2O)_2]$ was calculated as 536 $Å^3$ per unit cell, 8.1% of the total unit cell volume. Before removal, the interstitial water molecules were calculated to occupy 640.8 $Å^3$ per unit cell, or 9.3% of the unit cell volume. These values are comparable to those observed for the $[Cu(\mathbf{L_{ala}})_2(4,4'\text{-bipy})(H_2O)_2]\cdot 4.25H_2O$ complex.

These dehydration processes can also be followed in detail by thermogravimetric analysis (TGA). When $[Cu(\mathbf{L_{ala}})_2(4,4'\text{-bipy})(H_2O)_2]\cdot 4.25H_2O$ is heated to decomposition, two peaks can be observed below 150 °C in the differential weight loss curve (Figure 15): one at 46 °C, which corresponds to the interstitial water molecules (ca. 8.1% observed weight loss, 7.5% calculated), and a second, smaller one at 120 °C, which is assigned to the loss of the coordinated water molecules. Above 200 °C, the sample starts to decompose.

If the sample is not heated above 100 °C, the dehydration process is reversible. A crystalline sample of $[Cu(\mathbf{L_{ala}})_2(4,4'\text{-bipy})(H_2O)_2]\cdot 4.25H_2O$ was heated to 100 °C; in this process, the sample lost only the interstitial water molecules. After heating to 100 °C, the sample was allowed to cool to room

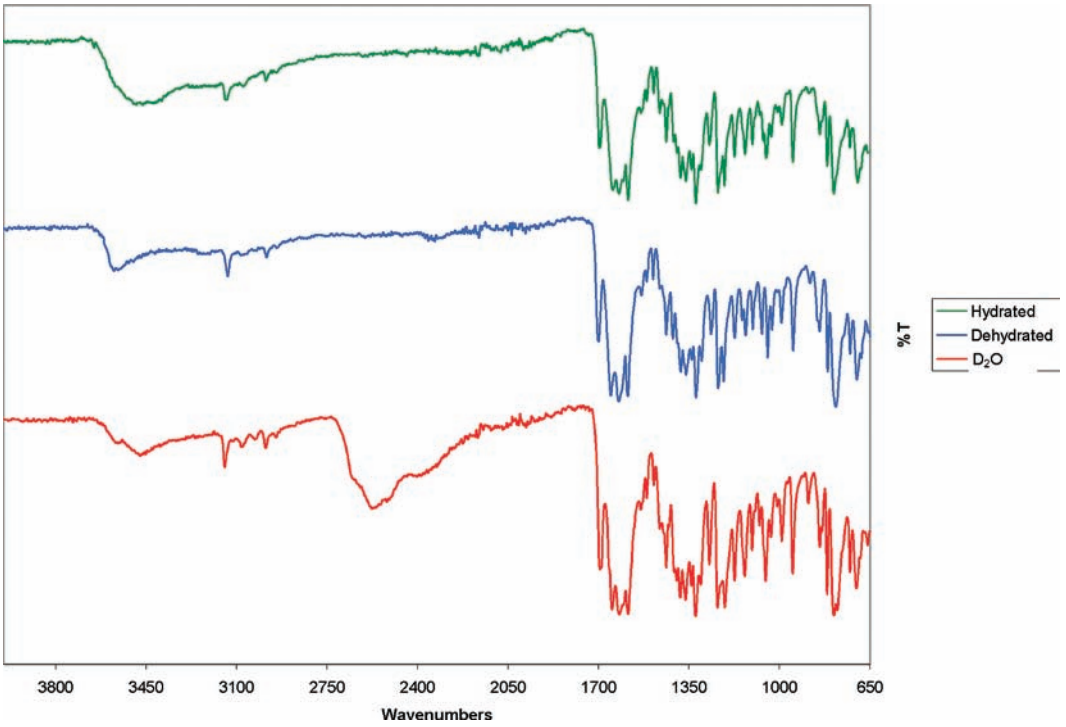

Figure 14. IR spectra of $[Cu(\mathbf{L_{ala}})_2(4,4'\text{-bipy})(H_2O)_2]\cdot 4.25H_2O$ (top, green), $[Cu(\mathbf{L_{ala}})_2(4,4'\text{-bipy})(H_2O)_2]$ (center, blue), and $[Cu(\mathbf{L_{ala}})_2(4,4'\text{-bipy})(H_2O)_2]\cdot 4.25D_2O$ (bottom, red).

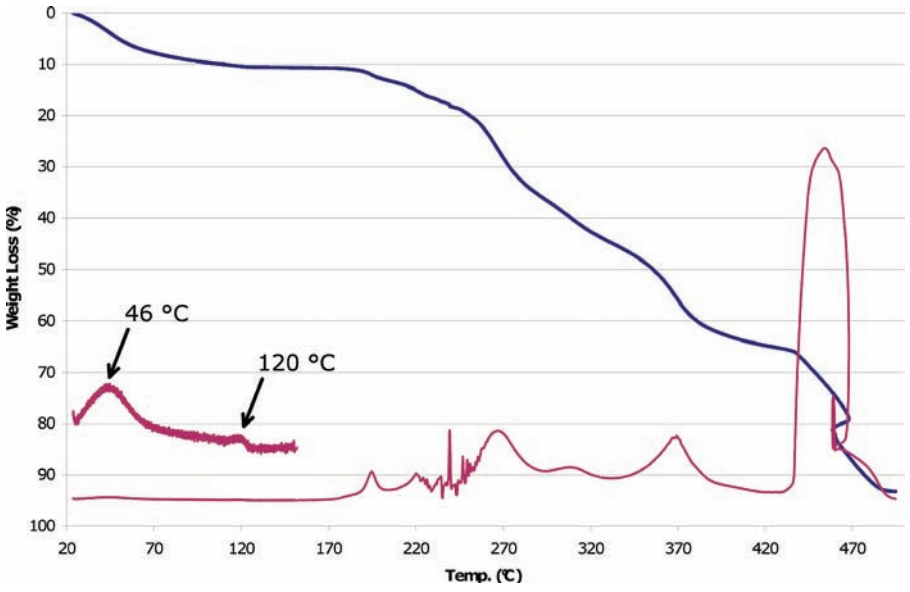

Figure 15. TGA plot for $[Cu(\mathbf{L_{ala}})_2(4,4'\text{-bipy})(H_2O)_2]\cdot 4.25H_2O$. The blue line corresponds to the percentage of weight loss upon heating, while the red is the derivative curve (arbitrary units). An expansion of the 25−150 °C section of the derivative curve is shown for clarity.

temperature and held there for an additional 22 h in ambient air inside the TGA chamber. Over this time period, a weight *gain* corresponding to the expected 4.25 mol of H_2O per unit was observed (Figure 16). This rehydrated sample was reheated and cooled by the same sequence, and the curve in Figure 16 was reproduced. In order to confirm that the sample had maintained its structure during dehydration/rehydration, powder X-ray diffraction was performed on ground crystals that had been dehydrated/rehydrated three times. As shown in the inset in Figure 16, the powder X-ray diffraction data on these crystals match the calculated patterns from the single-crystal X-ray data for $[Cu(\mathbf{L_{ala}})_2(4,4'\text{-bipy})(H_2O)_2]\cdot 4.25H_2O$, further demonstrating the robustness of the framework.

When heated to decomposition, the TGA curve for $[Co(\mathbf{L_{ser}})_2(4,4'\text{-bipy})(H_2O)_2]\cdot 4.68H_2O$ again shows two distinct peaks for the interstitial (65 °C) and coordinated (138 °C) water molecules (Figure 17). The interstitial peak, corresponding to a weight loss of ca. 8.3%, matches the calculated interstitial water mass (7.7%). Again, heating the sample to 100 °C drives off the interstitial water molecules, followed by cooling and exposure of the sample to ambient air, leads to rehydration of the sample. As in the case of $[Cu(\mathbf{L_{ala}})_2(4,4'\text{-bipy})(H_2O)_2]\cdot 4.25H_2O$, the powder X-ray diffraction pattern after

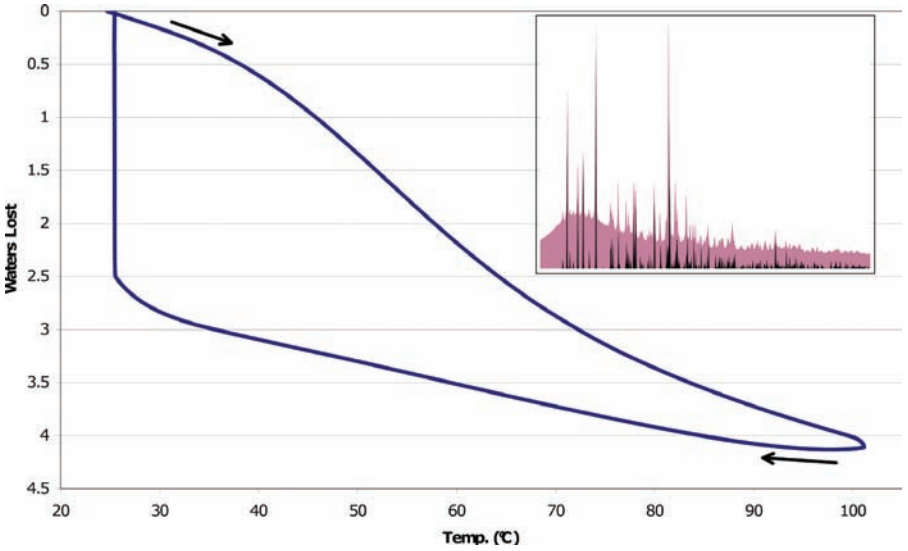

Figure 16. TGA curve (temperature vs number of H_2O lost) for dehydration and rehydration of $[Cu(\mathbf{L_{ala}})_2(4,4'\text{-bipy})(H_2O)_2]\cdot 4.25H_2O$. Inset: Comparison of the experimental (red) and calculated (black) powder X-ray diffraction patterns.

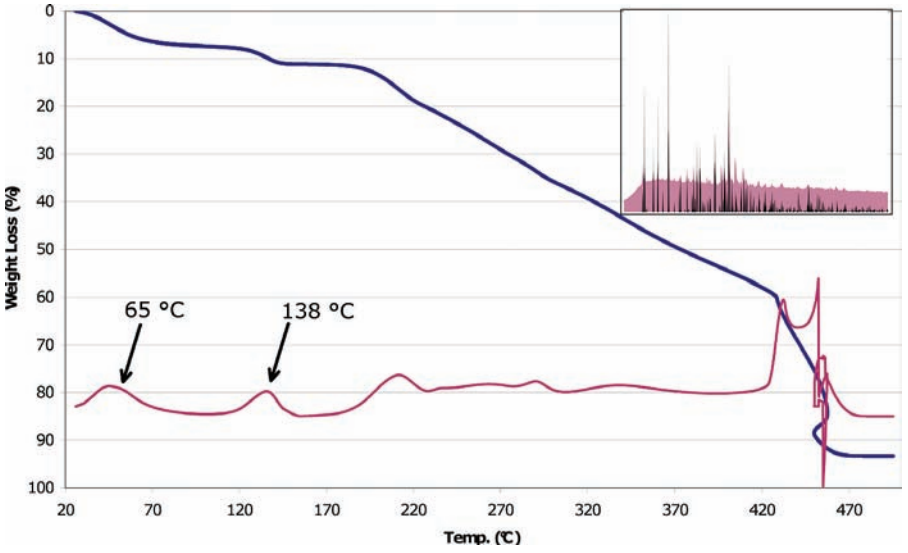

Figure 17. TGA curve for $[Co(\mathbf{L_{ser}})_2(4,4'\text{-bipy})(H_2O)_2]\cdot 4.76H_2O$. Inset: Comparison of the experimental (red) and calculated (black) powder X-ray diffraction patterns for samples that had been heated to 100 °C and rehydrated in ambient air three times.

three cycles of dehydration and rehydration matches the pattern calculated from the single crystals (Figure 17).

Surprisingly, even a steady stream of dry air at room temperature was sufficient to partially dehydrate both complexes. After 15 h of exposure to a steady stream of compressed air (at a flow rate of 100 mL/min), $[Cu(\mathbf{L_{ala}})_2(4,4'\text{-bipy})(H_2O)_2]\cdot 4.25H_2O$ had lost ~3.3 mol of H_2O per unit, while $[Co(\mathbf{L_{ser}})_2(4,4'\text{-bipy})(H_2O)_2]\cdot 4.76H_2O$ had only lost ~2.4 mol of H_2O per unit. This result indicates that, as expected, the serine-derived complex (with its additional hydrogen bonds) displays a greater affinity for water.

Magnetic Properties. As would be expected from the structures discussed above, even in the presence of the 4,4′-bipyridine-bridging ligands, all of the complexes under study are essentially magnetically dilute and exhibit paramagnetic Curie−Weiss law behavior [except those of diamagnetic zinc(II)] between 50 to 300 K for the iron(II) and cobalt(II) complexes or between 2 or 5 and 300 K for the nickel(II) and copper(II) complexes. As a result, the inverse molar magnetic susceptibilities, $1/\chi_M$, of the iron(II), nickel(II), and copper(II) complexes have been fit with the Curie−Weiss law (see the insets in Figures 18−21) to yield the Weiss temperatures, θ, Curie constants, C, and corresponding effective magnetic moments, μ_{eff}, given in Table 5. In contrast, because of the large temperature-independent contribution to χ_M present in the cobalt(II) complexes, their magnetic properties have been fit with a modified Curie−Weiss law, $\chi_M = \chi_{M,0} + C/(T-\theta)$, where $\chi_{M,0}$ is usually designated as $N\alpha$, the second-order Zeeman contribution to χ_M. For all of the complexes, the values shown in Table 5 are typical of the spin and oxidation states of the metal ion present.

At lower temperatures, all of the complexes exhibit a small decrease in $\chi_M T$ and μ_{eff}, a decrease that, except for the copper(II) complex, may be due to a combination of zero-field splitting, D, and/or a small amount of long-range magnetic exchange coupling, zJ. Thus, except for the copper(II) complex, the observed $\chi_M T$ has been

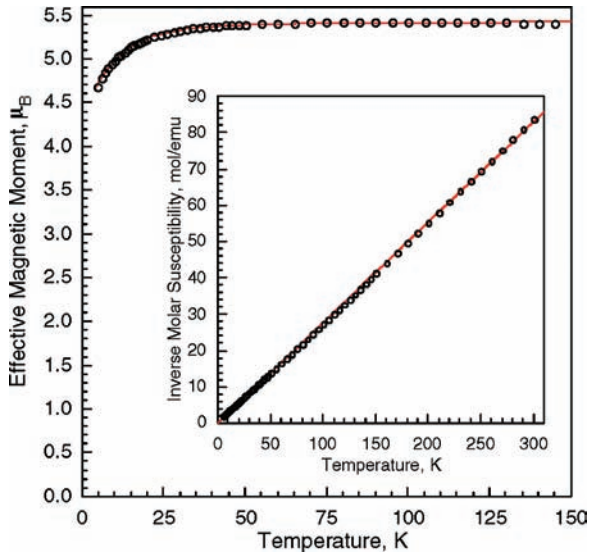

Figure 18. Temperature dependence of μ_{eff} of [Fe($\mathbf{L}_{ala}$)$_2$(4,4′-bipy)(H$_2$O)$_2$]·4.84H$_2$O, where the red 5−150 K fit of $\chi_M T$ with $S = 2$ yields $D = -8.44(7)$ cm^{-1} and $g = 2.215(1)$. Inset: Temperature dependence of $1/\chi_M$ and a Curie−Weiss law fit from 50 to 300 K.

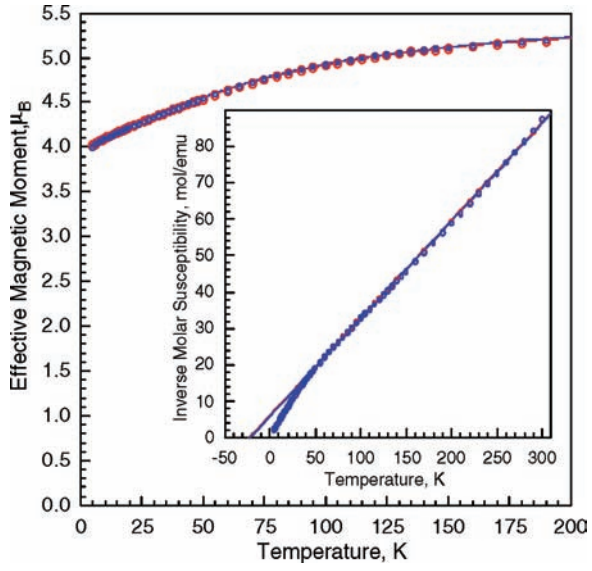

Figure 19. Temperature dependence of μ_{eff} of [Co($\mathbf{L}_{ala}$)$_2$(4,4′-bipy)(H$_2$O)$_2$]·4.76H$_2$O (blue) and [Co($\mathbf{L}_{ser}$)$_2$(4,4′-bipy)(H$_2$O)$_2$]·4.68H$_2$O (red), where the 5−200 K fit of $\chi_M T$ with $S = {}^3/_2$ in blue corresponds to $D = \pm 84(1)$ cm^{-1}, $zJ = -0.04(1)$ cm^{-1}, $N\alpha = 0.00118(3)$ emu/mol, and $g = 2.664(4)$ and the fit in red corresponds to $D = \pm 87(1)$ cm^{-1}, $zJ = -0.06(1)$ cm^{-1}, $N\alpha = 0.00100(3)$ emu/mol, and $g = 2.677(3)$. Inset: Temperature dependence of $1/\chi_M$ and a Curie−Weiss law fit from 50 to 300 K. In both plots, the fits virtually overlap.

fit[40] by adjusting D, zJ, $N\alpha$, and g, the Lande factor; the resulting parameters are given in Table 6, and the corresponding fits in terms of μ_{eff} are shown in the main portions of Figures 18−21. The fits revealed that no zJ or $N\alpha$ terms were needed to reproduce the observed decreases at lower temperature in the iron(II) and nickel(II) complexes. Further, in these complexes, a negative D value gave a somewhat better fit than a positive D value. In contrast, a perfect fit of the observed $\chi_M T$ for the copper(II) complex was obtained with small but very reasonable zJ and $N\alpha$ values. In all of these cases, the parameters, including the D values, are quite acceptable for the coordination environment observed about the metal ion.

As may be observed in Table 6, the fits of the observed $\chi_M T$ for the two cobalt(II) complexes require both D values to be approximately 10 times larger in magnitude than the remaining complexes and substantial $N\alpha$ values. Further, the positive and negative D values yield identical fits. As is discussed[41] by Kahn, this difference results

(40) O'Connor, C. J. *Prog. Inorg. Chem.* **1982**, *29*, 203.

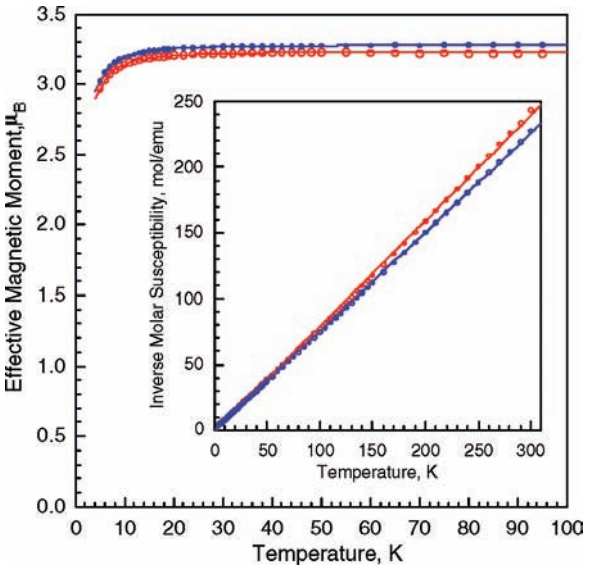

Figure 20. Temperature dependence of μ_{eff} of [Ni($\mathbf{L}_{ala}$)$_2$(4,4′-bipy)(H$_2$O)$_2$]·4.82H$_2$O (blue) and [Ni($\mathbf{L}_{ser}$)$_2$(4,4′-bipy)(H$_2$O)$_2$]·4.83H$_2$O (red), where the 5−100 K fit of $\chi_M T$ with $S = 1$ in blue corresponds to $D = -7.79(2)$ cm^{-1} and $g = 2.318(1)$ and the fit in red corresponds to $D = -7.99(4)$ cm^{-1} and $g = 2.284(1)$. Inset: Temperature dependence of $1/\chi_M$ and a Curie−Weiss law fit from 2 to 300 K.

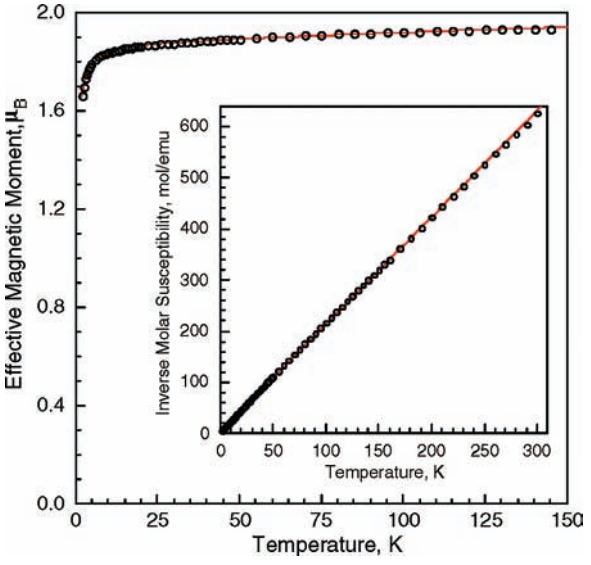

Figure 21. Temperature dependence of μ_{eff} of [Cu($\mathbf{L}_{ala}$)$_2$(4,4′-bipy)(H$_2$O)$_2$]·4.25H$_2$O, where the 2−150 K fit of $\chi_M T$ with $S = {}^1/_2$ in red corresponds to $zJ = -0.077(1)$ cm^{-1}, $N\alpha = 0.000201(4)$ emu/mol, and $g = 2.171(1)$. Inset: Temperature dependence of $1/\chi_M$ and a Curie−Weiss law fit from 2 to 300 K.

(41) Kahn, O. *Molecular Magnetism*; VCH Publishers, Inc.: New York, 1993; p 42.

Table 5. Curie−Weiss Law Parameters

metal/ligand	χ_M, corr, emu/mol	applied field, T	temp range, K	θ, K	C, emu K/mol	μ_{eff}, μ_B	g
Fe/$\mathbf{L_{ala}}^-$	−0.000 596	0.1	50−300	2.5	3.572	5.34	2.18
Co/$\mathbf{L_{ala}}^{-a}$	−0.000 594	0.1	50−300	−0.39	2.116	4.11	2.12
Ni/$\mathbf{L_{ala}}^-$	−0.000 595	0.1	5−300	0.26	1.328	3.26	2.30
Cu/$\mathbf{L_{ala}}^-$	−0.000 587	0.05	2−300	−2.50	0.479	1.96	2.26
Zn/$\mathbf{L_{ala}}^-$	−0.000 581	0.1	5−300		∼0	∼0	
Co/$\mathbf{L_{ser}}^{-b}$	−0.000 625	0.1	50−300	−0.39	2.126	4.12	2.13
Ni/$\mathbf{L_{ser}}^-$	−0.000 627	0.1	5−300	1.54	1.246	3.16	2.23

[a] Obtained from a modified Curie−Weiss law fit with $\chi_{M,0}$ = 0.007875 emu/mol. [b] Obtained from a modified Curie−Weiss law fit with $\chi_{M,0}$ = 0.007713 emu/mol.

Table 6. Magnetic Parameters[a]

metal/ligand	temp range, K	g	D, cm^{-1}	zJ, cm^{-1}	$N\alpha$, emu/mol
Fe/$\mathbf{L_{ala}}^-$	5−150	2.215(1)	−8.44(7)	0	0
Co/$\mathbf{L_{ala}}^-$	5−200	2.664(4)	±84(1)	−0.04(1)	0.001 18(3)
Ni/$\mathbf{L_{ala}}^-$	5−100	2.318(1)	−7.79(2)	0	0
Cu/$\mathbf{L_{ala}}^-$	2−150	2.171(1)		−0.077(1)	0.000 201(4)
Co/$\mathbf{L_{ser}}^-$	5−200	2.677(3)	±87(1)	−0.06(1)	0.001 00(3)
Ni/$\mathbf{L_{ser}}^-$	5−100	2.284(1)	−7.99(4)	0	0

[a] Obtained from fits of $\chi_M T$ over the specified temperature range. The statistical errors are shown, and the actual errors are expected to be much larger.

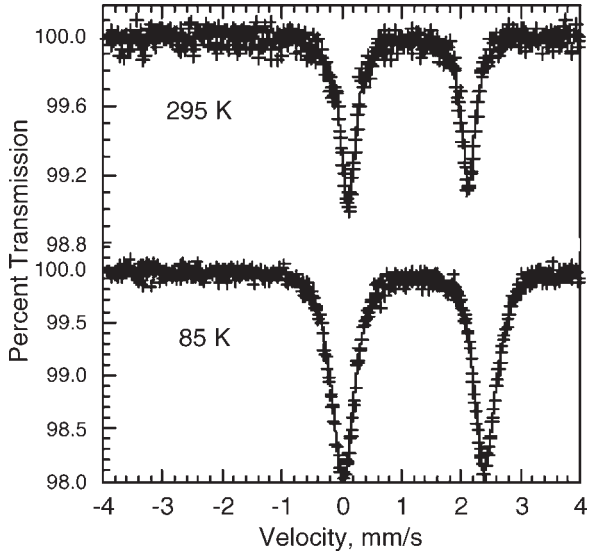

Figure 22. Mössbauer spectra of [Fe($\mathbf{L_{ala}}$)$_2$(4,4′-bipy)(H$_2$O)$_2$]·4.84H$_2$O obtained at the indicated temperatures. The intermediate temperature spectra are very similar.

because, for cobalt(II), the observed D value is actually a pseudo-D value that results from the thermal population of the two lowest Kramers doublets, Γ_6 and Γ_7, that arise from the $^4A_{2g}$ state of cobalt(II) in the presence of a sufficiently large crystal field. Complete details of these analyses are given in the Supporting Information.

Mössbauer Spectral Properties. The Mössbauer spectra of [Fe($\mathbf{L_{ala}}$)$_2$(4,4′-bipy)(H$_2$O)$_2$]·4.84H$_2$O have been measured between 85 and 295 K and fit with a single quadrupole doublet with one line width and slightly different component areas, a difference that is indicative of a small amount of texture in the absorber. Some of the resulting spectra are shown in Figure 22, and the fitted parameters are given in Table 7; the temperature dependence of the parameters is shown in Figure S1, and the results are discussed in detail in the Supporting Information. At all temperatures, the spectra are characteristic of a paramagnetic high-spin iron(II) complex with a quadrupole splitting that is typical of the axially

Table 7. Mössbauer Spectral Parameters for [Fe($\mathbf{L_{ala}}$)$_2$(4,4′-bipy)(H$_2$O)$_2$]·4.84H$_2$O

T, K	δ,[a] mm/s	ΔE_Q, mm/s	Γ, mm/s	absolute area (% ε) (mm/s)
295	1.118	2.02	0.29	0.935
225	1.154	2.13	0.33	1.240
155	1.181	2.20	0.36	1.718
85	1.213	2.38	0.43	2.523

[a] The isomer shifts are given relative to 295 K α-iron powder.

distorted octahedral iron(II) coordination environment observed in the structure of [Fe($\mathbf{L_{ala}}$)$_2$(4,4′-bipy)(H$_2$O)$_2$]·4.84H$_2$O. In view of the unique iron(II) crystallographic site found in [Fe($\mathbf{L_{ala}}$)$_2$(4,4′-bipy)(H$_2$O)$_2$]·4.84H$_2$O, the rather broad observed line widths of 0.29−0.43 mm/s are unexpected; the comparable FeSO$_4$·5H$_2$O spectra exhibit line widths of 0.23−0.25 mm/s between 295 and 85 K. The broadened line width presumably represents a small distribution in the quadrupole splitting, a distribution that results from a partial, perhaps random, loss of some of the 4.84 mol of the interstitial water of hydration found in the crystal structure of [Fe($\mathbf{L_{ala}}$)$_2$(4,4′-bipy)(H$_2$O)$_2$]·4.84H$_2$O. As discussed above, TGA results indicate that these solvation molecules may be easily lost and/or reabsorbed.

Discussion

An isostructural series of 12 homochiral, supramolecular helical MOF structures, formed by three different trifunctional ligands built from amino acids and bonded to five different first-row transition-metal ions, has been prepared and structurally analyzed. As anticipated from the design of the system, metal complexes of a long, flexible, enantiopure (in all but one complex) carboxylate ligand bearing a 1,8-naphthalimide group in combination with the rigid 4,4′-bipyridine linker produce homochiral framework structures supported in one direction *entirely by* $\pi\cdots\pi$ *stacking*. The coordinate−covalent bonding of the bridging 4,4′-bipyridine ligand, coupled with additional $\pi\cdots\pi$ stacking and hydrogen-bonding interactions, supports the other two dimensions of these densely packed structures. While many other studies

have combined hydrogen bonding with more classical "rigid" linkers,[21,42,43] the compounds reported here are unusual in mixing strong $\pi\cdots\pi$ stacking forces, forces previously calculated to be nearly as strong as hydrogen-bonding forces,[22] with classical "rigid" linkers.

The overall structures of these complexes show a remarkable insensitivity to the nature of the amino acid side chain. The same framework structure is formed when the amino acid side chain is changed from hydrogen ($\mathbf{L_{gly}}^-$) to methyl ($\mathbf{L_{ala}}^-$), despite the considerably greater steric bulk of the methyl group. The complex formed by the achiral ligand $\mathbf{L_{gly}}^-$ crystallizes as two separate enantiomorphs, one containing *P* helices and the other *M* helices. By using L-amino acids to build the ligands in the other structures, the *P* helix is observed in all 11 structures built from enantiopure ligands. The helical structure persists even when changing from $\mathbf{L_{ala}}^-$ to $\mathbf{L_{ser}}^-$, a change that introduces even more steric bulk, as well as the potential to form additional hydrogen bonds. The fact that the metal complex of achiral $\mathbf{L_{gly}}^-$ crystallizes in chiral space groups, a clear example of spontaneous resolution,[39] indicates that the basic shape of these new ligands, when combined with the strong $\pi\cdots\pi$ stacking ability of the 1,8-naphthalimide synthon, supports homochiral helical structures, with the handedness of the helix decided for the enantiopure ligands by the orientation of the chiral center.

It is the geometric orientation of the 1,8-naphthalimide interaction that directs the most notable structural feature of the framework, the large helical $\pi\cdots\pi$-stacked chains. These helical structures arise in spite of the nearly linear arrangement of the trans-coordinated carboxylate ligands because in each $\pi\cdots\pi$ stacking interaction the naphthalimide dipole vectors are oriented approximately 65° to one another. These $\pi\cdots\pi$ stacking interactions are strong. As shown in Table 3, the rings are nearly parallel with short plane−plane distances between them, the classical metric parameters quoted for strong $\pi\cdots\pi$ stacking.[15a] In addition, the parameter χ, a measure of "slippage" between the two rings, averages only 0.60 Å across all complexes, indicating a substantial overlap of the faces of the rings. For comparison, in our previous papers,[16,22] we observed slippage in the range between 0.60 and 2.4 Å for complexes that were considered to have strong interactions. Clearly, the small slippage values observed here coupled with the short plane−plane distances and the nearly parallel planes of the rings indicate strong interactions in these complexes. The strength of the naphthalimide $\pi\cdots\pi$ stacking interaction is also indicated by the structural stability of the frameworks.

The structural stability is dramatically demonstrated by the single-crystal to single-crystal transformation studies. Despite the densely packed structures, the interstitial water molecules can be removed by simply placing the crystals under vacuum. They can also be removed by heating and by placing the crystals in a stream of dry air. The ease of removal of the interstitial water molecules is surprising given that they are located in isolated pockets with no available "escape" channels and, with the exception of the partially occupied site, are strongly hydrogen-bonded to the helices (see Table 4). Only a few examples of nonporous compounds are known to undergo single-crystal to single-crystal gas/solid transformations.[42] The change is dramatic for the $[Cu(\mathbf{L_{ala}})_2(4,4'\text{-bipy})(H_2O)_2]\cdot 4.25H_2O$ complex because of the color change but was also clearly demonstrated by X-ray crystallography for the $[Co(\mathbf{L_{ser}})_2(4,4'\text{-bipy})(H_2O)_2]\cdot 4.68H_2O$ complex. The TGA studies show that the water molecules are more slowly removed, or removed at higher temperatures, from $[Co(\mathbf{L_{ser}})_2(4,4'\text{-bipy})(H_2O)_2]\cdot 4.68H_2O$. Given the additional hydrogen-bonding interactions with the serine CH_2OH side chain with the interstitial water molecules observed, this result is not surprising. What is surprising is that the interstitial waters can be *removed* at all from these closely packed solids without degradation of the crystalline structure.

The key to removal of the water molecules without disruption of the closely packed structure *must* lie in the "*soft*" $\pi\cdots\pi$ stacking interactions that organize the one dimension of the structures. As has been pointed out elsewhere,[38,43] structures such as those reported herein organized by both rigid and weaker linkages can have "local distortions" that allow the guests to migrate in or out of the structures. In previous cases of framework structures partially organized by softer interactions, removal of the guest molecules has generally led to pronounced structural changes,[44] changes *not* observed in the structures of the complexes reported here. The hydrated structures of these new complexes are densely packed with no void spaces other than the pockets that hold the interstitial water molecules. The structures of the dehydrated complexes change very little, other than containing void spaces where the water molecules had previously resided in the hydrated structures. Thus, the strong $\pi\cdots\pi$ stacking of the 1,8-naphthalimide groups seem to provide an unusual example in chemistry of having "the best of both worlds". That is, the $\pi\cdots\pi$ stacking provides substantial structure to the organization of the solid but also allows it to "breathe" such that the water molecules can be readily removed and reintroduced so that single-crystal to single-crystal transformations can be observed. Of course, the overall structures are organized by many other forces, mainly coordinate covalent bonding, but what appears unique in these complexes is the impact of the $\pi\cdots\pi$ stacking 1,8-naphthalimide synthon.

The magnetic properties of the complexes reported herein and the Mössbauer parameters of $[Fe(\mathbf{L_{ala}})_2(4,4'\text{-bipy})(H_2O)_2]\cdot 4.84H_2O$ are typical for isolated divalent octahedral first-row transition-metal complexes. While there is considerable

(42) Mobin, S. M.; Srivastava, A. K.; Mathur, P.; Lahiri, G. K. *Inorg. Chem.* **2009**, *48*, 4652.

(43) (a) Kitagawa, S.; Uemura, K. *Chem. Soc. Rev.* **2005**, *34*, 109–119. (b) Ding, B.; Weng, Y.; Mao, Z.; Lam, C.; Chen, X.; Ye, B. *Inorg. Chem.* **2005**, *44*, 8836–8845. (c) Kumar, D. K.; Das, A.; Dastidar, P. *New J. Chem.* **2006**, *30*, 1267–1275. (d) Di Nicola, C.; Karabach, Y. Y.; Kirillov, A. M.; Monari, M.; Pandolfo, L.; Pettinari, C.; Pombeiro, A. J. *Inorg. Chem.* **2007**, *46*, 221–230. (e) Liu, J.; Wang, Y.; Zhang, Y.; Liu, P.; Shi, Q.; Batten, S. R. *Eur. J. Inorg. Chem.* **2009**, *2009*, 147–154. (f) Halder, G. J.; Kepert, C. J. *Aust. J. Chem.* **2006**, *59*, 597.

(44) (a) Chen, B.; Ma, S.; Zapata, F.; Fronczek, F. R.; Lobkovsky, E. B.; Zhou, H. *Inorg. Chem.* **2007**, *46*, 1233–1236. (b) Tanaka, D.; Nakagawa, K.; Higuchi, M.; Horike, S.; Kubota, Y.; Kobayashi, T.; Takata, M.; Kitagawa, S. *Angew. Chem., Int. Ed.* **2008**, *120*, 3978–3982. (c) Horcajada, P.; Serre, C.; Maurin, G.; Ramsahye, N. A.; Balas, F.; Vallet-Regí, M.; Sebban, M.; Taulelle, F.; Férey, G. *J. Am. Chem. Soc.* **2008**, *130*, 6774–6780. (d) Chen, B.; Liang, C.; Yang, J.; Contreras, D. S.; Clancy, Y. L.; Lobkovsky, E. B.; Yaghi, O. M.; Dai, S. *Angew. Chem., Int. Ed.* **2006**, *118*, 1418–1421. (e) Férey, G.; Serre, C. *Chem. Soc. Rev.* **2009**, *38*, 1380–1399. (f) Suh, M. P.; Moon, H. R.; Lee, E. Y.; Jang, S. Y. *J. Am. Chem. Soc.* **2006**, *128*, 4710–4718. (g) Fletcher, A. J.; Thomas, K. M.; Rosseinsky, M. J. *J. Solid State Chem.* **2005**, *178*, 2491–2510.

interest in the magnetic properties of homochiral systems,[45] the compounds reported here are not chiral at the metal ions; thus, the chirality built into the backbone of the ligands does not appear to greatly impact these properties.

Acknowledgment. The authors acknowledge with thanks the financial support of the U.S. National Science Foundation through Grant CHE-1011736 and of the "Fonds National de la Recherche Scientifique," Belgium through grants 9.456595 and 1.5.064.05.

(45) Train, C.; Gheorghe, R.; Krstic, V.; Chamoreau, L.-M.; Ovanesyan, N. S.; Rikken, G. L. J. A.; Gruselle, M.; Verdaguer, M. *Nat. Mater.* **2008**, *7*, 729.

Supporting Information Available: X-ray crystallographic files in CIF format for the structural determinations and details of magnetic and Mössbauer spectral analysis. This material is available free of charge via the Internet at http://pubs.acs.org.